Chemie Ingenieur Technik

Models for the Numerical Simulation of Bubble Columns: A Review

Adam Mühlbauer, Mark W. Hlawitschka, and Hans-Jörg Bart*

DOI: 10.1002/cite.201900109

This work reviews the state-of-the-art models for the simulation of bubble columns and focuses on methods coupled with computational fluid dynamics (CFD) where the potential and deficits of the models are evaluated. Particular attention is paid to different approaches in multiphase fluid dynamics including the population balance to determine bubble size distributions and the modeling of turbulence where the authors refer to numerous published examples. Additional models for reactive systems are presented as well as a special chapter regarding the extension of the models for the simulation of bubble columns with a present solid particle phase, i.e., slurry bubble columns.

Keywords: Bubble column reactors, Breakup and coalescence, CFD simulation, Multiphase modeling, Solid-particle effect

Received: July 26, 2019; *revised:* October 15, 2019; *accepted:* October 16, 2019

1 Introduction

Bubble columns are widely applied in chemical, petrochemical, biochemical and metallurgical processes [1–3]. As to this, they are of special research interest as outlined in the *Chemie Ingenieur Technik* Special Issue "Campus Blasensäulen" [4]. In bubble columns, two or more phases depending on the process coexist. The dispersed gas phase leads to a high gas-liquid interfacial area. The continuous phase may be a liquid, an emulsion or a slurry. In heterogeneously catalyzed processes, solid particles with different properties, like size and shapes, can be present. The reactions are, e.g., oxidation, chlorination, alkylation, polymerization and hydrogenation [5, 6]. An overview of industrial processes performed in bubble columns is given by Schlüter et al. [7]. Despite the widespread applications of bubble columns, the interactions between hydrodynamics, mass transfer mechanisms, chemical reactions, yield and product quality are inadequately known so far.

The big advantage of bubble columns is their simplicity with respect to construction and usually the absence of moving parts results in low maintenance costs. The turbulent flow inside the apparatus allows for excellent heat and mass transfer, however, large backmixing is a disadvantage. The complex fluid dynamics are further influenced by breakage and coalescence of the bubbles, which affect reactor performance. Numerous experimental investigations on the gas holdup in different fluid systems can be found, where a detailed overview of investigated bubble column processes is given by Leonard et al. [8].

The design of the columns is often based on simplified integral models that are not able to account for the complex interactions between local fluid dynamics, mass transfer, reactions, heat transfer and material properties. Among the factors affecting gas-liquid mass transfer rates Sideman et al. [9] reported:

- physical properties of gas and liquid,
- gas flow rate,
- gas holdup,
- bubble size (distributions),
- bubble velocity or relative slip velocity,
- presence of solid catalyst,
- presence of chemical reaction, concentration of electrolytes,
- type of distributor, orifice diameter, spacing and position,
- dimensions of column or tank, baffles.

Sideman et al. [9] concluded that the large number of factors makes the design based on a single correlation impossible. The elements can be evaluated by multiscale analyses paired with simulations and will lead to a more accurate and resource efficient column design.

In fact, strong progress has been made within the last 30 years to simulate bubble columns with CFD methods. The results are partially implemented in available commercial or open source CFD software today. Important reviews can be found in literature describing the success and limitations of numerical bubble column simulations. Tomiyama [10] presents the early work of computational bubble dynamics. The basic approaches for the simulation of bubbly flows are presented in detail, which still form the basis of simulations coupled with CFD today. Jakobsen et al. [11] address the

Adam Mühlbauer, Dr.-Ing. habil. Mark W. Hlawitschka,
Prof. Dr. techn. Hans-Jörg Bart
bart@mv.uni-kl.de
Technische Universität Kaiserslautern, Lehrstuhl für Thermische Verfahrenstechnik, Gottlieb-Daimler-Straße 44, 67663 Kaiserslautern, Germany.

importance of boundary conditions formulation, turbulence modeling and bubble breakup and coalescence. Especially, a modeling of the latter is not straightforward. Wang [12] reviews the CFD approach coupled with a population balance model, which is capable of predicting the complex fluid dynamics in the homogeneous and heterogeneous regime and the bubble size distribution (BSD). But there are still difficulties with turbulence modification when simulating systems at high gas holdup. Furthermore, industrial systems are operated at high pressures and temperatures, they may contain solid particles (e.g., as a catalyst) or there are varying fluid properties. The models partially lack to account for the occurring phenomena in these systems. In addition, reactions can take place and in general all the described processes are strongly coupled and affect each other.

In contrast to the basic flow sheet modeling, the simulation of bubble columns using CFD enables a description of the fluid dynamics, the ongoing interactions and reactive mass transfer and, thus, lead to a to a better understanding of the effects in bubble columns. Furthermore, CFD helps to identify suitable correlations and, therefore, leads to a better and optimized scale-up of the columns. The data derived from numerical simulations may be also used to close the step towards digitalization by obtaining validated correlations for multiphase apparatuses.

This article presents the basic approaches and gives an overview over reliable models for the simulation of bubble columns, which were applied successfully within the past years. Different approaches to simulate bubbly flows and the mathematical formulation of the models are collated in this work. A special section focuses on the modeling of solid-particle effects in bubble columns. Emphasis is put on the necessities for further research and development where the main chances are evaluated.

2 Two-Phase Systems

Approaches to simulate the flow and phase interactions are presented in this section where the focus lies on the strong coupling of the phases in gas-liquid flows.

2.1 Direct Numerical Simulation

Steady-state and transient simulations of single bubbles enable an isolated investigation of effects such as bubble rise, shape and oscillation. Thereby, the influence of interacting bubbles on the bubble rise [13, 14], the changes by surfactants [15–17] and mass transfer [18–21] can be studied and correlations for coarse-scale modeling can be obtained. For the direct numerical simulation (DNS) of bubbly flows, a one-fluid approach is commonly used to describe the fluid dynamics [22, 23]:

$$\frac{\partial \rho}{\partial t} + \nabla \cdot (\rho \mathbf{u}) = 0 \tag{1}$$

$$\begin{aligned} &\frac{\partial \rho \mathbf{u}}{\partial t} + \nabla \cdot (\rho \mathbf{u} \otimes \mathbf{u}) = -\nabla p + (\rho - \rho_0)\mathbf{g} \\ &+ \nabla \cdot \left(\nabla \mathbf{u} + (\nabla \mathbf{u})^{\mathrm{T}} \right) + \sigma \kappa \delta(n) \mathbf{n} \end{aligned} \tag{2}$$

with the mean density $\rho_0 = \alpha_g \rho_g + (1 - \alpha_g)\rho_l$.

The computational techniques for capturing the interface were improved over the years and led to higher accuracy [24]. The 2D investigations of bubble swarms were continuously transferred to 3D cases [25–28]. Methods for interface capturing and related examples are listed in Tab. 1.

2.2 Euler-Euler Approach and Population Balance Modeling

The Euler-Euler approach (EE) considers all fluids as interpenetrating continua. The degree of detail is lower than in DNS and closure laws as well as other models to account for the dynamics of bubbles of different sizes become necessary.

2.2.1 Two-Fluid Model

To describe the flow of the fluids the conservation equations of mass and momentum are solved for each phase (i = gas, liquid) [49].

$$\frac{\partial (\alpha_i \rho_i)}{\partial t} + \nabla \cdot (\alpha_i \rho_i \mathbf{u}_i) = 0 \tag{3}$$

$$\begin{aligned} &\frac{\partial (\alpha_i \rho_i \mathbf{u}_i)}{\partial t} + \nabla \cdot (\alpha_i \rho_i \mathbf{u}_i \otimes \mathbf{u}_i) \\ &= -\alpha_i \nabla p + \nabla \cdot (\alpha_i \tau_i) + \alpha_i \rho_i \mathbf{g} + \mathbf{F}_i^{\mathrm{inter}} \end{aligned} \tag{4}$$

The stress tensor τ includes the turbulent stresses and can be written as

$$\tau = \mu^{\mathrm{eff}} \left(\nabla \mathbf{u} + (\nabla \mathbf{u})^{\mathrm{T}} - \frac{2}{3} I (\nabla \cdot \mathbf{u}) \right) \tag{5}$$

μ^{eff} is the effective viscosity and may include the turbulent viscosity μ^{turb} and a term due to bubble-induced turbulence μ^{BIT}. The phase volume fractions fulfill the constraint:

$$\sum_i \alpha_i = 1 \tag{6}$$

For the interphase exchange terms cumulated within $\mathbf{F}_i^{\mathrm{inter}}$ a multitude of combinations can be found in literature. Rzehak and Kriebitzsch [49] suggest with their so-called baseline model the following forces for bubbly flows:

$$\mathbf{F}_g^{\mathrm{inter}} = -\mathbf{F}_i^{\mathrm{inter}} = \mathbf{F}^{\mathrm{drag}} + \mathbf{F}^{\mathrm{lift}} + \mathbf{F}^{\mathrm{wall}} + \mathbf{F}^{\mathrm{disp}} \tag{7}$$

Table 1. Different DNS methods for gas-liquid flows.

Method	Advantages	Disadvantages	Investigations	Related work
Front tracking	extremely accurate, robust	mapping of interface mesh onto Eulerian mesh, remeshing required, moderate *Re* and *Sc* numbers, 2D case	deformable interface, bubble swarms, bubbly flow (up to 9 bubbles) with mass transport in non-Newtonian media, 2D and 3D simulations	Esmaeeli & Tryggvason [22, 29] Tryggvason et al. [30] Radl et al. [31]
Level set	conceptually simple, easy implementation	limited accuracy, employment of a mass conservation scheme required	rising bubble, deformation of a droplet	Sethian [32] Chang et al. [33] Sussman et al. [34] Croce et al. [35]
Shock capturing	straightforward implementation, abundance of advection schemes is available	numerical diffusion, fine grids		Ida [36]
Marker particles	accurate, robust, introduction of tagged Lagrangian particles as interface	computationally expensive, redistribution of marker particles required	bubble-obstacle interactions	Welch et al. [37], Hlawitschka et al. [38]
Simple line interface calculation (SLIC) VOF	conceptually simple	numerical diffusion, limited accuracy		Noh & Woodward [39]
Piecewise linear interface calculation (PLIC) VOF	relatively simple, accurate	difficult to implement, requires adaption to be suitable for unstructured meshes		Rider & Kothe [40] Ito et al. [41] Huang et al. [42]
Isosurface reconstruction VOF	species transport and interface reconstruction	dynamic mesh refinements required	interfacial mass transfer	Deising et al. [43]
Lattice Boltzmann	accurate, enables to account for interface changes	introduction of antidiffusion sweep to prevent mixing of the phases or direct geometrical interface representation required, problems with nonuniform meshes	particle drag of solid (nondeformable) spheres (cylinders), deformable bubbles: drag and virtual mass coefficient closure	Ladd [44, 45] Janssen & Krafczyk [46] Sankaranarayanan et al. [47] Sankaranarayanan & Sundaresan [48]

The effective drag force is often corrected to $\mathbf{F}^{\mathrm{drag,eff}} = C_{\mathrm{swarm}}\mathbf{F}^{\mathrm{drag}}$ to take swarm effects into account. Also, the added-mass or virtual mass force $\mathbf{F}^{\mathrm{vm}}$ can be applied in bubble column simulations [50] and is frequently found in literature. Expressions and correlations applied in published bubble column simulations can be found in Tab. 2.

The closures in Tab. 2 were mostly applied for air-water systems and could be validated with experimental results. For industrial systems with different fluid properties, models still have to be validated with experiments. Further material systems have to be defined covering – or at least representing some of – the wide range of industrial applications and validate the simulation models with well-defined, standardized experimental setups. In addition, one would also wish to find studies on the effects of the combinations of different models to get a more harmonized way of modeling bubble columns for different flow regimes and column dimensions.

2.2.2 Population Balance Equation

The bubble diameter plays an important role in the closures presented in Sect. 2.2.1 and is strongly coupled with the flow regime. A common way to resolve the bubble size distribution is by solving the population balance equation (PBE). The volume-based formulation for the number density function n of bubble volumes V is:

Table 2. Applied phase interaction closures for bubbly flows.

Term	Correlation	Ref.
Drag force		
$\mathbf{F}^{\text{drag}} = -C_{\text{D}}\alpha_{\text{g}}\frac{3}{4d_{\text{b}}}\rho_{\text{l}}\lvert\mathbf{u}_{\text{g}}-\mathbf{u}_{\text{l}}\rvert \times (\mathbf{u}_{\text{g}}-\mathbf{u}_{\text{l}})$	$C_{\text{D}} = \begin{cases}\frac{24}{Re}\left(1+0.15Re^{0.687}\right), & Re \le 1000\\ 0.44, & Re > 1000\end{cases}$	Schiller & Naumann [51]
	$C_{\text{D}} = \max\left[C_{\text{D,sph}}, \min\left[C_{\text{D,ell}}, C_{\text{D,cap}}\right]\right]$	Grace et al. model [52]
	with $C_{\text{D,sph}} = \begin{cases}\frac{24}{Re}, & Re < 0.01\\ \frac{24(1+0.15Re^{0.687})}{Re}, & 0.01 \le Re\end{cases}$, $C_{\text{D,ell}} = \frac{4}{3}\frac{gd_{\text{b}}}{u_{\text{t}}^2}\frac{\rho_{\text{l}}-\rho_{\text{g}}}{\rho_{\text{l}}}$, $C_{\text{D,cap}} = \frac{8}{3}$ and $u_{\text{t}} = \frac{\mu_{\text{l}}}{d_{\text{b}}\rho_{\text{l}}}Mo^{-0.149}(J-0.857)$, $J = \begin{cases}0.94H^{0.757}, & 2 < H \le 59.3\\ 3.42H^{0.441}, & 59.3 < H\end{cases}$, $H = \frac{4}{3}EoMo^{-0.149}\left(\frac{\mu_{\text{l}}}{9\cdot 10^{-4}\,\text{Pa s}}\right)^{-0.14}$	
	$C_{\text{D}} = \max\left[\frac{24}{Re}\left(1+0.15Re^{0.75}\right), \min\left[\left(\frac{2}{3}\sqrt{Eo}\right), \frac{8}{3}\right]\right]$	Ishii & Zuber [53]
	$C_{\text{D}} = \max\left[\frac{24}{Re}\left(1+0.15Re^{0.687}\right), \frac{8}{3}\frac{Eo}{Eo+4}\right]$	Tomiyama et al. [54]
	$C_{\text{D}} = \begin{cases}\frac{16}{Re}, & Re < 1.5\\ 14.9Re^{-0.78}, & 1.5 < Re < 80\\ \frac{48}{Re}\left(1-2.21Re^{-0.5}\right)+1.86\cdot 10^{-15}Re^{4.756}, & 80 < Re < 1500\\ 2.61, & 1500 < Re\end{cases}$	Laín et al. [55]
	$C_{\text{swarm}} = \left(1-\alpha_{\text{g}}\right)^{-0.5}$	Tomiyama et al. [56]
	$C_{\text{swarm}} = \exp\left(3.64\alpha_{\text{g}}\right)+\alpha_{\text{g}}^{0.864}$	Rusche & Issa [57]
	$C_{\text{swarm}} = \left(1+\frac{18}{Eo}\alpha_{\text{g}}\right)\left(1-\alpha_{\text{g}}\right)$	Roghair et al. [58]
Lift force		
$\mathbf{F}^{\text{lift}} = C_{\text{L}}\alpha_{\text{g}}\rho_{\text{l}}\left(\mathbf{u}_{\text{l}}-\mathbf{u}_{\text{g}}\right) \times \text{rot}(\mathbf{u}_{\text{l}})$	$C_{\text{L}} = \sqrt{\left\{C_{\text{l}}^{\text{lowRe}}\right\}^2+\left\{C_{\text{l}}^{\text{highRe}}\right\}^2}$	Legendre & Magnaudet [59]
	with $C_{\text{l}}^{\text{lowRe}} = \frac{6}{\pi^2}(ReSr)^{-0.5}\left(\frac{2.255}{\left(1+0.2\frac{Re}{Sr}\right)^{1.5}}\right)$ and $C_{\text{l}}^{\text{highRe}} = \frac{1}{2}\frac{1+16Re^{-1}}{1+29Re^{-1}}$	
	$C_{\text{L}} = \begin{cases}\min[0.288\tanh(0.121Re), f(Eo_{\perp})], & Eo_{\perp} < 4\\ f(Eo_{\perp}), & 4 < Eo_{\perp} < 10\\ -0.27, & 10 < Eo_{\perp}\end{cases}$	Tomiyama et al. [60]
	with $f(Eo_{\perp}) = 0.00105Eo_{\perp}^3 - 0.0159Eo_{\perp}^2 - 0.0204Eo_{\perp} + 0.474$	
	Models for aspect ratio $E_{\text{b}} = \frac{d_{\text{b}\parallel}}{d_{\text{b}\perp}}$:	
	$E_{\text{b}} = \frac{1}{1+0.163Eo^{0.757}}$	Wellek et al. [61]
	$E_{\text{b}} = \begin{cases}1, & Ta \le 1\\ \left(0.81+0.206\tanh\left(1.6-2\log_{10}Ta\right)\right)^3, & 1 < Ta \le 39.8\\ 0.24, & 39.8 < Ta\end{cases}$	Vakhrushev & Efremov [62]

Table 2. continued

Term	Correlation	Ref.
Wall lubrication force		
$\mathbf{F}^{\text{wall}} = C_{\text{W}}\alpha_{\text{g}}\frac{2}{d_{\text{b}}}\rho_{\text{l}}\lvert\mathbf{u}_{\text{l}}-\mathbf{u}_{\text{g}}\rvert^2\hat{\mathbf{y}}$	$C_{\text{W}} = \max\left[0, \frac{C_{\text{w1}}}{d_{\text{b}}}+\frac{C_{\text{w2}}}{y_{\text{w}}}\right]$	Antal et al. [63]
	with $C_{\text{w1}} = -0.01$ and $C_{\text{w2}} = 0.05$	
	$C_{\text{W}} = C_{\text{w3}}\frac{d_{\text{b}}}{2}\left(\frac{1}{y_{\text{w}}^2}-\frac{1}{(D_{\text{col}}-y_{\text{w}})^2}\right)$	
	$C_{\text{w3}} = \begin{cases} 0.47, & Eo < 1 \\ \exp(-0.933Eo+0.179), & 1 \le Eo \le 5 \\ 0.00599Eo-0.0187, & 5 < Eo \le 33 \\ 0.179, & 33 < Eo \end{cases}$	Tomiyama [10]
	$C_{\text{w3}} = \max\left[\frac{7}{Re^{1.9}}, 0.0217Eo\right]$	Hosokawa et al. [64]
	$C_{\text{w3}} = \max\left[\frac{0.1}{C_{\text{wd}}}\frac{1-\frac{y_{\text{w}}}{C_{\text{wc}}d_{\text{b}}}}{y_{\text{w}}\left(\frac{y_{\text{w}}}{C_{\text{wc}}d_{\text{b}}}\right)^{\text{P}_{\text{w}}-1}}\right]$	Frank [65]
	with $C_{\text{wc}} = 10.0$, $C_{\text{wd}} = 6.8$, and $p_{\text{w}} = 1.7$	
Turbulent dispersion		
$\mathbf{F}^{\text{disp}} = -C_{\text{TD}}\rho_{\text{l}}k_{\text{l}}\nabla\alpha_{\text{g}}$ (Lahey et al. [66])	$C_{\text{TD}} = 0.1$	Lucas et al. [68]
$\mathbf{F}^{\text{disp}} = -C_{\text{D}}\alpha_{\text{g}}\frac{3}{4d_{\text{b}}}\lvert\mathbf{u}_{\text{l}}-\mathbf{u}_{\text{g}}\rvert\frac{\mu_{\text{l}}^{\text{turb}}}{\sigma_{\text{TD}}} \times\left(\frac{1}{\alpha_{\text{l}}}+\frac{1}{\alpha_{\text{g}}}\right)\nabla\alpha_{\text{g}}$ (Burns et al. [67])	$C_{\text{TD}} = C_{\mu}^{1/4}\frac{1}{St(1+St)}$	Lopez de Bertodano et al. [69, 70]
	$\sigma_{\text{TD}} = 0.9$	Rzehak & Kriebitzsch [49]
Virtual mass		
$\mathbf{F}^{\text{vm}} = C_{\text{VM}}\alpha_{\text{g}}\rho_{\text{l}}\left(\frac{\text{D}\mathbf{u}_{\text{l}}}{\text{D}t}-\frac{\text{D}\mathbf{u}_{\text{g}}}{\text{D}t}\right)$	$C_{\text{VM}} = 0.5$	Zhang et al. [71, 72]

$Re = \frac{\rho_{\text{l}}\lvert\mathbf{u}_{\text{g}}-\mathbf{u}_{\text{l}}\rvert d_{\text{b}}}{\mu_{\text{l}}}$, $Eo = \frac{g\left(\rho_{\text{l}}-\rho_{\text{g}}\right)d_{\text{b}}^2}{\sigma}$, $Eo_{\perp} = Eo(d_{\text{b}} = d_{\text{b}\perp})$, $Mo = \frac{\mu_{\text{l}}^4 g\left(\rho_{\text{l}}-\rho_{\text{g}}\right)}{\rho_{\text{l}}^2\sigma^3}$, $Sr = Re_{\omega}/Re$, $Re_{\omega} = \frac{\rho_{\text{l}}\lvert\text{rot}(\mathbf{u}_{\text{l}})\rvert d_{\text{b}}^2}{\mu_{\text{l}}}$, $Ta = ReMo^{0.23}$, D/Dt: material derivative.

$$\begin{aligned}&\frac{\partial n(V)}{\partial t}+\nabla\cdot\left(\mathbf{u}_{\text{g}}n(V)\right)\\&=\underbrace{\int_{\text{V}}^{\infty}\nu_{\text{b}}(V')\beta_{\text{b}}(V,V')g_{\text{b}}(V')n(V')\text{d}V'-g_{\text{b}}(V)n(V)}_{\text{S}_{\text{breakup}}}\\&+\underbrace{\frac{1}{2}\int_{0}^{\text{V}}\Gamma_{\text{c}}(V-V',V')n(V-V')n(V')\text{d}V'-n(V)\int_{0}^{\infty}\Gamma_{\text{c}}(V,V')n(V')\text{d}V'}_{\text{S}_{\text{coalescence}}}\end{aligned}\tag{8}$$

with $\Gamma_{\text{c}}(V,V') = \lambda_{\text{c}}(V,V')h_{\text{c}}(V,V')$ for coalescence of bubbles with volumes V and V'.
The source terms for breakup and coalescence in Eq. (8) are crucial for the determination of bubble diameters.

Breakup and Coalescence Models

Models for the breakage frequency g_b and daughter size distribution β_b are required to simulate breakup. The coalescence frequency Γ_c exists of the collision frequency h_c and the coalescence efficiency λ_c. These quantities are related to the fluid and flow properties. Some models applicable for bubbly flows are listed in Tabs. 3 and 4.

Most of the models for the breakage frequency are based on the assumption of bubbles colliding with turbulent eddies, but there are also concepts of breakup due to viscous shear stresses or surface instabilities [81]. In literature, mainly binary breakup of bubbles can be found, which is described by the daughter size distribution, but the models for the latter differ. A good overview is given by Liao and Lucas [81].

The mechanisms for collision are turbulent motion, velocity gradients, buoyancy and wake-entrainment [82]. In general, the model for the coalescence efficiency

$$\lambda_c = \exp\left(-\frac{t_{ij}}{\tau_{ij}}\right) \tag{9}$$

depends on the ratio of the film drainage time t_{ij} and the contact time τ_{ij}. The assumptions for the models are immobile, partially mobile or fully mobile gas-liquid interfaces.

Solution Methods

Various numerical schemes can be used to solve Eq. (8). An overview is given in Tab. 5. The major difference between the solution methods is within the information about the BSD. With the moment-based and one-group models the information about the actual BSD is lost and only mean values like the Sauter mean diameter can be calculated. But in return, the computing time decreases with the latter methods and gets close to the computing time required for pure fluid dynamic calculations. Though, BSD can be reconstructed with various assumptions.

A peculiarity for the simulation of BSD can be found with the developed GENTOP-concept, where large bubbles are modeled as a continuous phase and interact with a discrete method for smaller bubbles [104]. With this concept it is possible to simulate also complex flow structures with high gas fractions.

Visualization and Validation

One of the main drawbacks of EE is the loss of the exact particle position and shape. The bubbles are finally described by the phase fraction and a field of particle sizes. A direct link in visualization is mainly missing and makes a comprehensive explanation and comparison to visual experimental observations to non-CFD experts a challeng-

Table 3. Applicable breakup models for bubble column simulations.

Breakage frequency g_b	Daughter size distribution β_b	Ref.
$g_b = \int_{0.2d_b}^{d_b} \frac{0.07\pi^4}{\lambda_\varepsilon}(d_b+\lambda_\varepsilon)^2\left(d_b^{2/3}+\lambda_\varepsilon^{2/3}\right)^{0.5}\varepsilon^{1/3} \times \exp\left(-\frac{1.18}{\lambda_\varepsilon^{2/3}}\frac{\sigma}{\rho_l d_b \varepsilon^{2/3}}\right)d\lambda_\varepsilon$	uniform	Prince & Blanch [73]
$g_b = \frac{1}{2}\int_0^1 0.923(1-\alpha_g)n\left(\frac{\varepsilon}{d_b^2}\right)^{1/3} \times \int_{\xi_{min}}^1 \frac{(1+\xi)^2}{\xi^{11/13}}\exp\left(-\frac{12c_f\sigma}{c_\beta\rho_l\varepsilon^{2/3}d_b^{5/3}\xi^{11/13}}\right)d\xi df_{bv}$	$\beta_b = \frac{2\int_{\xi_{min}}^1(1+\xi)^2\xi^{-11/3}\exp(-\chi_c)d\xi}{V_b\int_0^1\int_{\xi_{min}}^1(1+\xi)^2\xi^{-11/3}\exp(-\chi_c)d\xi df_{bv}}$	Luo & Svendsen [74]
with $\xi = \frac{\lambda_\varepsilon}{d_b}$, $c_f = f_{bv}^{2/3}+(1-f_{bv})^{2/3}-1$, $f_{bv} = \frac{d_{bi}^3}{d_{bi}^3+d_{bj}^3}$, $c_\beta = 2$	with $\chi_c = \frac{12c_f\sigma}{c_\beta\rho_l\varepsilon^{2/3}d_b^{5/3}\xi^{11/3}}$	
$g_b = \frac{1}{2}\int_0^1\int_{d_b'}^{d_b} 0.8413\sqrt{2}\frac{\sigma}{\rho_l\varepsilon^{2/3}d_b^{4}}\frac{(\lambda_\varepsilon-d_b)^2}{\lambda_\varepsilon^{13/3}\exp\left(-\frac{2\sigma}{\rho_l\varepsilon^{2/3}d_b\lambda_\varepsilon^{2/3}}\right)}d\lambda_\varepsilon df_{bv}$	$\beta_b = \frac{1}{\sqrt{\pi}f_{bv}}\frac{\exp\left(-\frac{9}{4}\left(\ln\left(\frac{2^{2/5}d_{ba}\rho_l^{3/5}\varepsilon^{2/5}}{\sigma^{\frac{3}{5}}}\right)\right)^2\right)}{1+\mathrm{erf}\left(\frac{3}{2}\ln\left(\frac{2^{1/15}d_{ba}\rho_l^{3/5}\varepsilon^{2/5}}{\sigma^{3/5}}\right)\right)}$	Lehr et al. [75]
$g_b = C_{g,L1}\varepsilon^{1/3}\mathrm{erfc}\left(\sqrt{C_{g,L2}\frac{\sigma}{\rho_l\varepsilon^{2/3}d_b^{5/3}}+C_{g,L3}\frac{\mu_l}{\sqrt{\rho_l\rho_g}\varepsilon^{1/3}d_b^{4/3}}}\right)$	$\beta_b = \left(9+\frac{33}{2}C_{\beta,L}+9C_{\beta,L}^2+\frac{3}{2}C_{\beta,L}^3\right) \times\left(\frac{d_{bi}^2}{d_{bj}^3}\right)\left(\frac{d_{bi}^3}{d_{bj}^3}\right)^2\left(1-\frac{d_{bi}^3}{d_{bj}^3}\right)^{C_{\beta,L}}$	Laakkonen et al. [76]

Table 4. Applicable coalescence models for bubble column simulations.

Collision frequency h_c	Coalescence efficiency λ_c	Ref.
$h_c = C_{h,CT}\frac{\varepsilon^{1/3}}{1+\alpha_g}\left(d_{bi}+d_{bj}\right)^2\left(d_{bi}^{2/3}+d_{bj}^{2/3}\right)^{0.5}$	$\lambda_c = \exp\left(-C_{\lambda,CT}\frac{\mu_l\rho_l\varepsilon}{\sigma^2\left(1+\alpha_g\right)^3}\left(\frac{d_{bi}d_{bj}}{d_{bi}+d_{bj}}\right)^4\right)$	Coulaloglou & Tavlarides [77]
$h_c = \underbrace{0.089\pi\varepsilon^{1/3}\left(d_{bi}+d_{bj}\right)^2\left(d_{bi}^{2/3}+d_{bj}^{2/3}\right)^{0.5}}_{\text{turbulence}}$ $+\underbrace{0.25\pi\left(d_{bi}+d_{bj}\right)^2\left\lvert u_{bi}-u_{bj}\right\rvert}_{\text{buoyancy-driven}}+\underbrace{\frac{1}{6}\left(d_{bi}+d_{bj}\right)^3\overline{\mathrm{d}u_l}/\mathrm{d}R}_{\text{laminar shear}}$ with $u_b=\left(\frac{2.14\sigma}{\rho_l d_b}+0.505 g d_b\right)^{0.5}$ and $\overline{\mathrm{d}u_l}/\mathrm{d}R$: average shear	$\lambda_c = \exp\left(-\frac{r_{bij}^{5/6}\rho_l^{0.5}\varepsilon^{1/3}}{4\sigma^{0.5}}\ln\left(\frac{h_0}{h_f}\right)\right)$ with $r_{bij}=0.5\left(\frac{1}{r_{bi}}+\frac{1}{r_{bj}}\right)^{-1}$, $h_0 = 10^{-4}$ m, $h_f = 10^{-8}$ m	Prince & Blanch [73]
$h_c = \frac{\pi}{4}\left(d_{bi}+d_{bj}\right)^2 n_i n_j\left(u_{bi}^2+u_{bj}^2\right)^{0.5}$	$\lambda_c = \exp\left(-C_{\lambda,Luo}\frac{\left(0.75\left(1+\left(\frac{d_{bi}}{d_{bj}}\right)^2\right)\left(1+\left(\frac{d_{bi}}{d_{bj}}\right)^3\right)\right)^{0.5}}{\left(\frac{\rho_g}{\rho_l}+C_{VM}\right)\left(1+\frac{d_{bi}}{d_{bj}}\right)^3}We_{ij}^{0.5}\right)$ with $C_{c,Luo} = 0.4$ for heterogenous flow and $We_{ij}=\frac{\rho_l d_b\left(u_{bi}^2+u_{bj}^2\right)}{\sigma}$	Luo [78]
$h_c^{turb} = 0.25\pi\frac{\alpha_{g,max}}{\alpha_{g,max}-\alpha_g}\exp\left(-\left(\frac{6.3\left(\frac{N_i}{\Delta d_i}+\frac{N_j}{\Delta d_j}\right)^{-1/3}}{0.89\sqrt{d_{bi}^2+d_{bj}^2}}\right)^6\right)$ $\times\sqrt{2}\varepsilon^{1/3}\left(d_{bi}+d_{bj}\right)^2\left(d_{bi}^{2/3}+d_{bj}^{2/3}\right)^{0.5}$ and $h_c^{wake} = c_{h,W}\Theta d_{bi}^2 0.71\sqrt{g d_{bi}}$ with $\Theta=\begin{cases}\frac{\left(d_j-\frac{d_c}{2}\right)^6}{\left(d_{bj}-\frac{d_c}{2}\right)^6+\left(\frac{d_c}{2}\right)^6}, & \frac{d_{bj}}{d_c}\geq 2,\ d_c = 4\sqrt{\frac{\sigma}{g\left(\rho_l-\rho_g\right)}}\\ 0, & \text{else}\end{cases}$	$\lambda_c = \exp\left(-C_{\lambda,HI}\sqrt[6]{\frac{\left(\frac{d_{bi}d_{bj}}{d_{bi}+d_{bj}}\right)^5\rho_l^3\varepsilon^2}{\sigma^3}}\right)$	h_c: Wang et al. [79] λ_c: Hibiki & Ishii [80]

ing task. Therefore, Hlawitschka et al. [95, 105–107] developed sampling strategies to visualize uncertain multiphase fluid simulation data. Based on the diameter and phase fraction fields, a representative number of bubbles and their location can be obtained, and the bubbles can be reconstructed as Lagrangian particles in a postprocessing step. The particle shape is reconstructed based on the dimensionless numbers *Eo* and *Re* and can be visualized, e.g., with the open source code VisIt. The specific particle volume is conserved and the generated Lagrangian particles are positioned that a direct overlap of the generated bubbles is prevented. An example is shown in Fig. 1.

The transfer of a Eulerian data set to a Lagrangian framework enables further postprocessing steps. One among the most promising is the comparing visualization [107]. The treatment of the data set as Lagrangian particles allows for a description of specific parameters moving with a fluid element, e.g., the contact time of a fluid element with the gas interfacial area. A set of simulations with different boundary conditions, e.g., the flow rate, can be further compared to each other using ensemble visualization, which puts the deviations of several simulations in a single plot.

2.3 Euler-Lagrange Approach

With the Euler-Lagrange approach (EL) the conservation equations for the continuous liquid phase prevail according to Eqs. (3) and (4). For every bubble the balance of forces is solved:

$$m_b\frac{\mathrm{d}\mathbf{u}_b}{\mathrm{d}t} = \sum_i \mathbf{F}_i \tag{10}$$

Table 5. Methods for discretization and solution of the PBE (Eq. (8)).

Classification	Method	Description	Related work
Discrete method	Homogeneous and inhomogeneous classes method (CM) - mixed pivot technique - moving pivot technique	Discretization of the population balance in a finite set of intervals. Solving momentum conservation equation for average of whole set of the interval (homogeneous method) or partially averaged intervals (inhomogeneous method). Information about BSD is available.	Hounslow et al. [83] Lister et al. [84] Ramkrishna [85] Chen et al. [86] Sanyal et al. [87] Frank et al. [88] Bhole et al. [89]
Moment-based Methods	Standard method of moments (SMM)	Transformation of the population balance to the transport of moments of the number density.	Hulburt & Katz [90]
	Quadrature method of moments (QMOM)	Quadrature approximation is applied to describe the moments. Well established method with drawbacks in product difference algorithm and ill-conditioning.	McGraw [91] Marchisio et al. [92] Lage [93]
	Direct quadrature method of moments (DQMOM)	Weights and abscissas are directly accounted in the transport equation.	Marchisio & Fox [94] Hlawitschka et al. [95]
	Conditional quadrature method of moments (CQMOM*)	Enabling a conditioning of the moment matrix.	Yuan & Fox [96]
	Cumulative quadrature method of moments (CQMOM*)	Tracking of the cumulative distribution.	Attarakih [97]
	Extended quadrature method of moments (EQMOM)	Approximation by a sum of non-negative weight functions	Yuan et al. [98] Mahvelati et al. [99]
	Sectional quadrature method of moments (SQMOM)	Section-wise approximation with QMOM.	Attarakih et al. [100] Schäfer et al. [101]
One-group models	One primary one secondary particle method (OPOSPM)	The simplest form of SQMOM. Conserves volume and number of particles. Short simulation times.	Attarakih et al. [102] Hlawitschka et al. [95]
	Interfacial area transport equation (IATE)	Transporting the interfacial area instead of number and size. Calculation of Sauter mean diameter. Low computational costs.	Hibiki & Ishii [80] Ishii et al. [103]

*The conditional QMOM and the cumulative QMOM were introduced at the same time in 2011.

where $\sum_i \mathbf{F}_i = m_b \frac{\rho_g - \rho_l}{\rho_g}\mathbf{g} + \frac{\mathbf{F}_g^{inter}}{\alpha_g}$ and $\mathbf{F}_g^{inter}$ are expressions according to Eq. (7) listed in Tab. 2.

Every bubble can be tracked by solving the equation of motion:

$$\frac{d\mathbf{x}_b}{dt} = \mathbf{u}_b \tag{11}$$

The computational effort depends strongly on the total number of bubbles in the domain [108], but more information about the disperse phase characteristics may be obtained than when using EE. With EL simulations it is possible to calculate the bubble pathways through the domain and the residence time distributions. In comparison to the first bubble column simulations in an EL framework [109–112] an improvement of the models is noticeable. Details of bubble movement, like bubble oscillations, can be simulated. Depending on the bubble size, velocity and fluid properties different motion patterns occur, like rectilinear, zigzag and helical motion [113]. Weber et al. [114] describe an approach to simulate bubble oscillations. They introduce a side force depending on the orientation of an ellipsoidal bubble whereby they solve the simplified Jeffery's equation. Bubble breakup and coalescence of the bubbles can be modeled stochastically [108, 115–117] and can be also

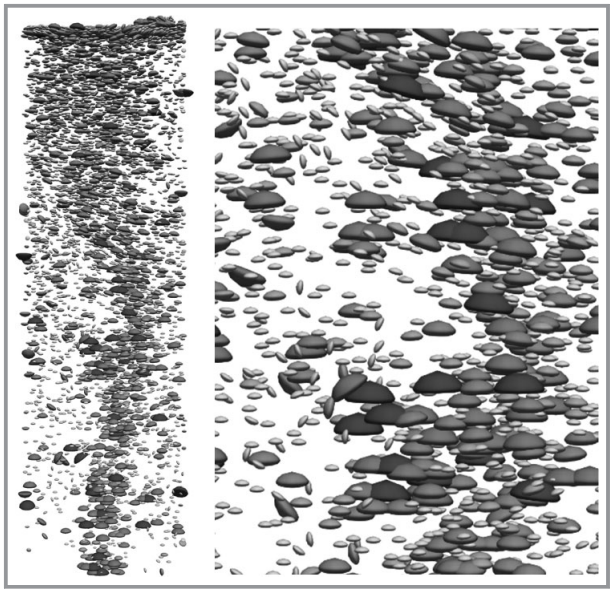

Figure 1. Bubbly flow visualization accounting for bubble orientation and bubble shape derived from data calculated with EE-SQMOM approach (left: bubble column, right: zoom).

accounted for the gas-liquid interface at the top of the column [118].

A limitation of EL is the predicament with the spatial resolution of the continuous phase domain because the cell size must not exceed bubble size excessively [10]. Sungkorn et al. [119] argue with a tolerable grid spacing to bubble diameter range of $0.5 < \Delta_S/d_b < 10$ if the total number of bubbles is small. An advanced approach to simulate bubbles larger than cell size comes with the immersed boundary methods, where coupling between the disperse and continuous phase is performed with a Lagrangian surface mesh [120].

2.4 Turbulence Modeling

The turbulent characteristics play an important role in bubble columns. There are different effects on radial and axial mixing as well as on BSD via breakup and coalescence as the models in Tabs. 3 and 4 indicate.

In literature, mostly Reynolds-averaged Navier-Stokes (RANS) turbulence models and large eddy simulations (LES) can be found [121]. Another peculiarity is bubble-induced turbulence (BIT), which has to be accounted. The formulations of the k and ε conservation equations are:

$$\frac{\partial(\alpha_l\rho_l k)}{\partial t} + \nabla\cdot\left(\alpha_l\rho_l\mathbf{u}_l k - \alpha_l\left(\mu_l + \frac{\mu_l^{\text{turb}}}{\sigma_k}\right)\nabla k\right) = \alpha_l(G - \rho_l\varepsilon) + S_k^{\text{BIT}} \tag{12}$$

$$\frac{\partial(\alpha_l\rho_l\varepsilon)}{\partial t} + \nabla\cdot\left(\alpha_l\rho_l\mathbf{u}_l\varepsilon - \alpha_l\left(\mu_l + \frac{\mu_l^{\text{turb}}}{\sigma_\varepsilon}\right)\nabla\varepsilon\right) = \alpha_l\left(C_{\varepsilon 1}\frac{\varepsilon}{k}G - C_{\varepsilon 2}\rho_l\frac{\varepsilon^2}{k}\right) + S_\varepsilon^{\text{BIT}} \tag{13}$$

with constants $\sigma_k = 1.0$, $\sigma_\varepsilon = 1.217$, $C_{\varepsilon 1} = 1.44$, $C_{\varepsilon 2} = 1.92$ and the production of turbulent kinetic energy $G = \tau_l : \nabla\mathbf{u}_l$ [71]. The shear-induced turbulent viscosity is

$$\mu_l^{\text{turb}} = C_\mu\rho_l\frac{k^2}{\varepsilon} \tag{14}$$

with $C_\mu = 0.09$.

LES sub-grid models (SGS) as proposed by Smagorinsky [122] are applied where

$$\mu_l^{\text{turb}} = \rho_l\left(C^{\text{SGS}}\Delta_S\right)^2|\mathbf{S}| \tag{15}$$

The Smagorinsky constant is of the order of magnitude $C^{\text{SGS}} = 0.1$ [123] but should rather be considered as a modeling parameter which can be adapted [124]. The filter width is $\Delta_S = (\Delta_x\Delta_y\Delta_z)^{1/3}$ and should be chosen so that $\Delta_S/d_b \approx 1.2$ applies [124].

A possible way to model the bubble-induced effects on turbulence is by considering the effective viscosity

$$\mu_l^{\text{eff}} = \mu_l + \mu_l^{\text{turb}} + \mu_l^{\text{BIT}} \tag{16}$$

with an additional model for the shear-induced viscosity [125]

$$\mu_l^{\text{BIT}} = \rho_l\alpha_g C_\mu^{\text{BIT}} d_b\left|\mathbf{u}_g - \mathbf{u}_l\right| \tag{17}$$

An overview of models also for the source terms S_k^{BIT} and $S_\varepsilon^{\text{BIT}}$ in Eqs. (12) and (13) to account for bubble-induced turbulence is listed in Tab. 6.

Recent investigations of Khan et al. [121] point out some weaknesses of the very often applied standard k-ε model for bubbly flows. They compared different k-ε and Reynolds stress models (RSM) with LES. Detailed experimental data for validation was taken from Bhole et al. [130]. They mention also poor performance of the k-ε model with bubble-induced turbulence. LES is computationally more expensive but can resolve transient effects like bubble plume motions and velocity fluctuations. However, care has to be taken when choosing the physical and numerical parameters because they may significantly affect the results [124]. Examples where LES was applied successfully for bubbly flows can be found in [131, 132]. Magolan et al. [133] compared a multitude of BIT models with experimental data from Liu [134]. They analyze the differences of the models and the deviations from the measurements. Parekh and Rzehak [135] investigated the anisotropy of bubble-induced turbulence with RSM and point out that further formulations for modeling turbulent effects should be explored. In the field of multiphase turbulence there is still a clear need for further research.

Table 6. Applicable terms for Eqs. (12) and (13) to model BIT.

BIT model	S_k^{BIT}	S_ε^{BIT}	μ_l^{BIT}
Sato & Sekoguchi [125]	0	0	Eq. (17)
Pfleger & Becker [126]	$\alpha_l C_k \left\lvert \mathbf{F}_l^{drag} + \mathbf{F}_l^{lift} + \mathbf{F}_l^{vm} \right\rvert \lvert \mathbf{u}_g - \mathbf{u}_l \rvert$ with $C_k = 1.44$	$\frac{\varepsilon}{k} C_\varepsilon S_k^{BIT}$ with $C_\varepsilon = 1.92$	0
Troshko & Hassan [127]	$\left\lvert \mathbf{F}_l^{drag} \right\rvert \lvert \mathbf{u}_g - \mathbf{u}_l \rvert$	$0.45 \frac{3 C_D \lvert \mathbf{u}_g - \mathbf{u}_l \rvert}{2 C_{VM} d_b} S_k^{BIT}$	0
Rzehak & Krepper [128]	$\mathbf{F}_l^{drag} \cdot (\mathbf{u}_g - \mathbf{u}_l)$	$C_{\varepsilon b} \frac{S_k^{BIT}}{\tau}$ with $C_{\varepsilon b} = 1.0$ and $\tau = \frac{d_b}{\sqrt{k}}$	0
Ma et al. [129]	$\min[0.18 Re^{0.23}, 1] \cdot \mathbf{F}_l^{drag} \cdot (\mathbf{u}_g - \mathbf{u}_l)$	$0.3 C_D \frac{S_k^{BIT}}{\tau}$	0

2.5 Chemical Reaction Modeling

The aforementioned simulation techniques focus on the fluid dynamic description of bubble columns. For process optimization and design, the final concentrations in the gaseous and liquid phases are of predominant importance, which were mainly calculated using flow sheet modeling while the uncertainty of the hydrodynamics prevailed. In recent years, CFD simulations were coupled with mass transfer and chemical reaction equations to describe the occurring interactions. The focus was on two-phase flows and mainly on the well described chemisorption of carbon dioxide in sodium hydroxide solution. As mentioned in Sect. 2.3, EL simulations can provide a high level of detail but also EE became popular due to a lower computational time and an improved description of the BSD due to population balance modeling and, therefore, to account also for a high gas holdup [136, 137]. In both approaches additional species transport equations have to be introduced. The following description is based on the EE approach, but can be also adapted to EL simulations [138, 139].

$$\frac{\partial\left(\alpha_l \rho_l Y_l^j\right)}{\partial t} + \nabla \cdot \left(\alpha_l \rho_l Y_l^j - \alpha_l \rho_l D_l^j \nabla Y_l^j\right) = \dot{m}_{g\to l}^j - \dot{m}_{l\to g}^j + \alpha_l \dot{S}_l^j \tag{18}$$

Only $N_S - 1$ transport equations are solved, where N_S corresponds to the number of species observed in the process and the mass fractions of the species must fulfill

$$\sum_{j=1}^{N_s} Y^j = 1 \tag{19}$$

The mass transfer can be based on the two-film theory, the surface renewal theory or the penetration theory.

In Fig. 2, Y_g^j and Y_l^j represent the mass fractions in the bulk of the dispersed and the surrounding liquid phase, respectively. $Y_g^{j^*}$ and $Y_l^{j^*}$ describe the corresponding mass fractions at the interface. Based on the assumption of a liquid-side mass transfer resistance, the mass transfer rate for absorption $\dot{m}_{g\to l}^j$ is given by:

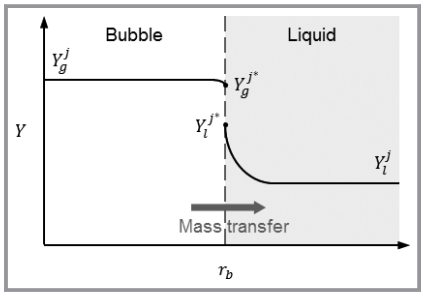

Figure 2. Mass transfer according to the two-film theory for absorption of a species in a gas bubble into the liquid bulk phase.

$$\dot{m}_{g\to l}^j = E k_l^j \frac{A}{V_{cell}} \rho_l \left(Y_l^{j^*} - Y_l^j\right) \tag{20}$$

where ρ_l is the density of the continuous phase, V_{cell} is the cell volume, and E is the enhancement factor that describes the influence of chemical reaction to the absorption. E can be derived from experiments or analytical expressions.

The interfacial area corresponds to the summation of the interface areas of each single bubble in a numerical cell. Assuming spherical bubbles of constant size, it corresponds to:

$$A = \frac{6}{d_b} \alpha_g V_{cell} \tag{21}$$

The mass transfer coefficient k_l^j is calculated based on the Sherwood number Sh^j and the diffusion coefficient D_l^j.

$$Sh^j = \frac{k_l^j d_b}{D_l^j} \tag{22}$$

For Sh^j empirical correlations can be found in literature [140].

$Y_l^{j^*}$ corresponds to the equilibrium mass fraction of species j in the liquid phase. It is defined by the Henry constant H.

$$H^j = \frac{c_l^{j^*}}{c_g^j} \tag{23}$$

Reactions describe the transformation of one set of chemical substances into another. The general stoichiometry equation of a reversible reaction for J species taking part in a reaction is:

$$\sum_{j=1}^{J_m'} \nu_m^{j'} X^j \rightleftharpoons \sum_{j=1}^{J_m''} \nu_m^{j''} X^j \tag{24}$$

X^j represents species j in the summation formula. $\nu_m^{j'}$ and $\nu_m^{j''}$ are the stoichiometric coefficients of the reaction m for the educt (left) and product side (right).

For a chemical system with M reactions the production rate $\dot{S}^j$ of a species j is:

$$\dot{S}^j = W^j \sum_{m=1}^{M} \left(\nu_m^{j''} - \nu_m^{j'}\right)\omega_m \tag{25}$$

The production rates $\dot{S}^j$ are the source terms in the species transport Eq. (18). The reaction velocity ω_m of the m-th reaction is dependent on the rate coefficients k_m' and k_m'' for the forward chemical reaction and the backward chemical reaction as well as on the concentrations c^j of the participating species j.

$$\omega_m = k_m' \prod_{j=1}^{J} \left(c^j\right)^{\nu_m^{j'}} - k_m'' \prod_{j=1}^{J} \left(c^j\right)^{\nu_m^{j''}} \tag{26}$$

The concentration c^j of the species j is derived from the mass fractions Y^j, the density ρ_l and the molar mass W^j:

$$c^j = Y^j \frac{\rho_l}{W^j} \tag{27}$$

3 Three-Phase Systems

The presence of solid particles in industrial processes, e.g., catalyzed reactions, complicates the simulation of bubble columns. The presented equations in Sect. 2 may be also applied to the simulation of slurry bubble columns with their basic features, but additional phenomena have to be considered. In the following, effects of solid particles in disperse three-phase systems will be discussed and modeling approaches are given.

3.1 Solid-Phase Effects

Solid particles may drastically affect the hydrodynamics in a column. It has been stated repetitiously that solid particles affect the gas holdup in an apparatus [141–143]. Also, correlations for the gas holdup for different compounds were derived and can be found collated in the work of Behkish et al. [144].

In addition, there are adverse solid-phase effects depending on the particle properties and arise mainly from different particle sizes. Particles with diameters in the submillimeter range, i.e., microparticles, mostly lead to a decrease whereas larger particles may increase the gas holdup [145]. The small particles change the slurry density and viscosity and promote bubble coalescence, where large bubbles decrease the gas holdup in slurry bubble columns [141, 142]. The promotion of coalescence was observed in the presence of hydrophobic [146] as well as of hydrophilic particles [147]. By contrast, large particles may lead to bubble breakage due to collisions [148]. This results in an increase of the gas holdup. In the following, only the influence of the technically more relevant microparticles will be evaluated.

Most of the investigations of these phenomena are of experimental nature and find dependencies on the present solid volume fraction [142, 149]. However, a gradient of solid volume fraction occurs in the axial direction in slurry bubble columns depending on fluidization or the superficial gas velocities. Also, different rising velocities of bubbles with equivalent diameters were observed with increased solid volume fraction [142]. It was also found that small particles can accumulate in the bubble wakes and increase their net mass force resulting in a lower relative velocity [150]. Additional drag on the bubbles may arise due to collisions with particles [151].

A last important point is the dissipation rate of turbulent kinetic energy ε, which is decreasing with the presence of small particles depending on the particle Stokes number and volume fraction [152]. Modeling approaches of the presented phenomena will be discussed in the Sect. 3.2.

3.2 Modeling Approaches

An overview of slurry bubble column simulations carried out with CFD methods can be found in Tab. 7. Nearly all recently published slurry bubble column simulations are carried out in a 3D domain, but different approaches exist when it comes to the modeling of phase interactions. Various schematics are depicted in Fig. 3.

Satisfying results can be obtained with various degrees of detail despite the focus of modeling may differ. Troshko and Zdravistch [156] applied a two-phase closure as depicted in Fig. 3a with the assumption of a perfectly mixed slurry. With this approach the solid-phase effects on the material properties of the continuous phase are taken into

Table 7. Selection of published slurry bubble column simulations.

Authors	CFD	Multiphase modeling	Population balance modeling	Experimental data for comparison	Peculiarities
Chen et al. [86]	3D	pseudo-2-phase	breakup/coalescence	own measurements	algebraic slip mixture model
Bourloutski & Sommerfeld [151]	3D	Euler/Lagrange	–	Michele et al. [153]	bubble-solid interactions
Matonis et al. [154]	3D	Euler multifluid	–	own measurements	solid-solid drag
Ojima et al. [147]	3D	Euler multifluid	breakup/coalescence	own measurements	solid-effect multiplier for coalescence
Rabha et al. [155]	3D	Euler multifluid	breakup/coalescence	own measurements	multiple size group model
Troshko & Zdravistch [156]	3D	2-phase Euler	breakup/coalescence	Krishna et al. [141], Kulkarni et al. [157]	perfectly mixed slurry, turbulence modification for breakup/coalescence, mass transfer
Wu & Gidaspow [158]	2D	Euler multifluid	–	Phenomenological and quantitative comparison with a variety of literature	heat and mass transfer
Xu et al. [159]	3D	pseudo-2-phase	breakup/coalescence	Gandhi et al. [160]	modified breakup/coalescence model
Zhang et al. [161]	pseudo-2D	Euler/Lagrange	coalescence	Delnoji et al. [162]	bubble-bubble and solid-solid collisions
Zhou et al. [163]	3D	Euler multifluid	–	Rados [164], Ojima et al. [147]	dual bubble size drag model

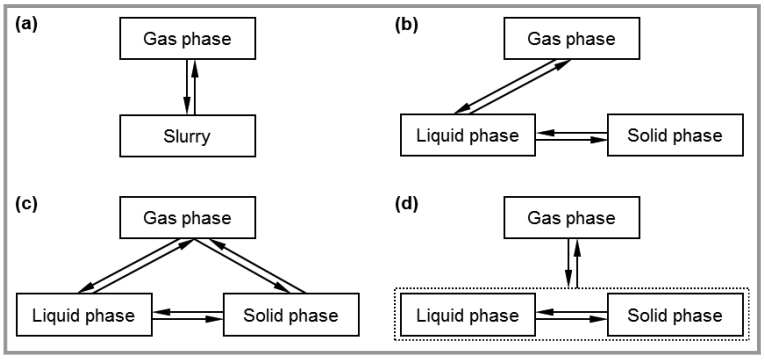

Figure 3. Interphase closures for gas-liquid-solid flows (adapted from Xu et al. [159]).

account. The slurry properties can be calculated according to Tsuchiya et al. [165]:

$$\rho_{sl} = (1-\alpha_s)\rho_l + \alpha_s\rho_s \tag{28}$$

$$\mu_{sl} = \mu_l \exp\left(\frac{C_s\alpha_s}{1-\frac{\alpha_s}{\alpha_{cs}}}\right) \tag{29}$$

with the constant parameters C_s and α_{cs} depending on the solid particle properties. Other possibilities are the consideration of single interactions between the gas and liquid phase as well as the liquid and solid phase (cf. Fig. 3b). But also bubble-solid collisions [151] or bubble-bubble and particle-particle collisions can be modeled [161].

Most frequently, the Euler multifluid approach is used with different closures for the interphase momentum exchange. One can regard an exchange between any possible combination of phases or reduced/hierarchical interphase momentum exchange as depicted in Figs. 3c and 3d [159]. It should be mentioned that also validated closures for the phase interactions of the solid particles have to be found in analogy to the models listed in Tab. 2. In all cases in Tab. 7 turbulence is modeled with RANS models of k-ε-type or is not mentioned.

Many authors modeled bubble breakup and coalescence, some even with the consideration of solid-phase effects, however, a lot of authors forgo the modeling of breakup and coalescence in their simulations. The solid effects are

missing in the breakage and coalescence models presented in Sect. 2.2.2. Different approaches to model the solid-phase effect on bubble breakup and coalescence can be found. So far, the three approaches are:

A) Adaption/fitting of breakup/coalescence parameters
B) Introduction of a solid-effect multiplier
C) Turbulence modification

A) With this approach, the bubble breakup and/or coalescence parameters are adapted to satisfy a certain condition and fit experimental data. In most of the cases this is a target quantity of measurements as well as the simulations, e.g., the total gas holdup [159], but to get a completely validated model, the spatial distribution of the quantities should be also considered. This ensures that the modeling deviations do not erase each other.

B) A solid-effect multiplier is introduced. The multiplier β accounts for the promotion of coalescence due to the presence of small solid particles and is considered in the expression for the coalescence efficiency [145, 147]:

$$\lambda_c^{se} = \exp\left(-\frac{\beta t_{ij}}{\tau_{ij}}\right) \tag{30}$$

where β may have values between 0 and 1 and can be deduced from film rupture measurements. Ojima et al. [166] carried out experiments in a quasi-2D column where they recorded the coalescence times with a high-speed camera with different particle volume fractions and diameters. The fitted correlations for β can be found in Fig. 4.

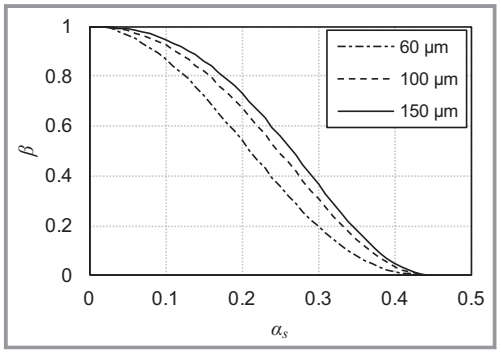

Figure 4. Solid-effect multiplier for different particle diameters (correlations from Ojima et al. [166]).

The solid-effect multiplier deduced from reference experiments can be also successfully applied with the Prince & Blanch coalescence model in CFD multifluid simulations [147]. Comparison between the simulations and experimental data indicate that the solid-effect multiplier approach gives better predictions for the gas holdup distribution in slurry bubble columns than without taking the solid effect into account.

C) Squires and Eaton [152] found that in dilute suspensions of particles the dissipation rate is attenuated. Troshko and Zdravistch [156] scaled the dissipation rate as an exponential function of the particle volume fraction based on DNS data from Squires and Eaton [152] according to

$$\frac{\varepsilon}{\varepsilon_0} = \exp(-C_{\varepsilon s}\alpha_s) \tag{31}$$

where ε_0 is the dissipation rate without the presence of particles. They modified the dissipation rate just for the calculation of the breakup and coalescence terms. The scaling approach is plotted in Fig. 5.

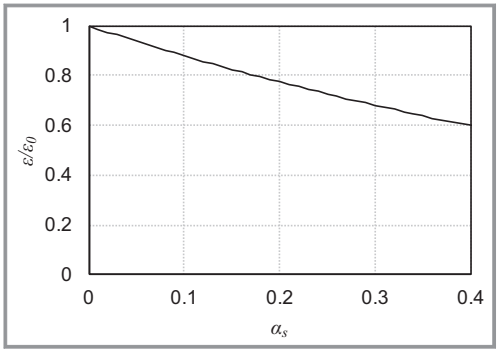

Figure 5. Dissipation rate modification according to Troshko and Zdravistch [156] for dilute systems and St = 0.14–0.5 based on DNS data from Squires and Eaton [152].

Troshko and Zdravistch [156] found that the modification of the dissipation rate as depicted in Fig. 5 is only valid for $\alpha_s \ll 1$ and $C_{\varepsilon s}$ has to be increased to fit experimental data for high solid volume fractions. The approach is based on physical investigations and addresses the turbulent dissipation in the three-phase system, but further investigations are required.

The presented approaches A) to C) improve the modeling of breakup and coalescence in slurry bubble columns. The phenomena addressed in approach B) and C) should be clarified before fitting the breakup and coalescence parameters to experimental data. The introduction of new model parameters would also be conceivable, which should be systematically investigated to account for different solid-particle properties. There is a need for research in the modeling of disperse three-phase systems, especially for the interphase closure models and the effects on breakup and coalescence. Numerical and experimental studies will help to find models with fluid dynamic quantities as well as material properties and should reduce the uncertainties implied by fitting parameters. Therefore, measurements are still essential to validate the simulations of slurry bubble columns.

4 Summary and Perspective

Within the last three decades, a lot of effort was put into the modeling and numerical simulation of bubble columns and substantial progress was made. Today, one can find a fundamental basis for the simulation of bubbly flows.

Single phenomena such as single bubbles rising and deforming can be simulated using DNS. EE and EL approaches can be applied to simulate a whole apparatus and large-scale flow. The main governing equations and the required closures were collected and presented in detail in Sect. 2. Also, the PBE was incorporated in this review, where special focus was on the applicable breakup and coalescence models as well as the discretization and solution methods of the PBE. The basic approaches for modeling turbulence and accounting for bubble-induced turbulence were presented in particular and the models were collated. However, there is in general still a need for research in the field of multiphase turbulence and for bubbly flow applications with high gas holdup. Within the last years, there was also a development towards the modeling of reactive bubble columns with the consideration of mass transfer. In heterogeneously catalyzed reactions, usually a solid catalyst is present. A special chapter in this work considered the effects of solid particles on the fluid dynamics, especially on breakup and coalescence of the bubbles. Various approaches to account for the solid-phase effects were presented and classified. However, physical approaches are not yet fully developed and almost all calculations are empirical in terms of the modeling of slurry bubble columns.

The models to simulate bubbly flows are advanced nowadays, though a lot of different closures can be found applied and validated in literature. Hardly any studies have been published on the interactions of the multitude of applicable models taking into account the full coupling of fluid dynamics and turbulence with population balance models. Targeted validation of single individual quantities becomes necessary. The same applies to simulations of industrial systems and with the presence of solid particles in particular.

The biggest opportunities to further reduce empirical design and bring the use of numerical simulation closer to practical applications lie in the systematic validation of the models. This should be supported with DNS on the small scale, where especially the transfer from single to bubble swarm models can be resolved in detail. In addition, closures for large-scale models can be deduced from DNS. For large-scale simulations, parameter sensitivity should be investigated and the dominant effects in the strongly coupled multiphase system identified. With CFD-coupled simulations a huge amount of data is generated, where also other methods like machine learning could be applied and used for column design and scale-up.

Nevertheless, experiments are still a necessary step for validation and extension of the modeling of multiphase flows. Therefore, standardized experiments should be defined to validate the description of particularly sensitive parameters, e.g., turbulence quantities, breakup and coalescence parameters and effects of impurities. Industry can participate in the definition of (representative) material systems and can set further research impulses to address their needs, e.g., the investigation of long-term effects such as foaming. Finally, an established database and a validated set of base models for a wide range of systems will considerably reduce the development times and uncertainty of developed models for process simulation.

The authors acknowledge the financial support from the Bundesministerium für Bildung und Forschung (BMBF) funded project "OptiMeOH" and the Deutsche Forschungsgemeinschaft (DFG) funded Research Training Group RTG 1932 "Stochastic Models for Innovations in the Engineering Sciences".

Adam Mühlbauer graduated at the University of Bayreuth in 2016 with specializations in environmental engineering and energy technology. During his studies, he started his work in the fields of multiphase flow modeling and experimental investigations of absorption processes. Since 2017, he is a PhD student at TU Kaiserslautern and investigates gas-liquid-solid flows where his main focus is on measurement and modeling of solid-particle effects in slurry bubble columns.

Mark W. Hlawitschka holds a PhD in process engineering for his work in liquid-liquid extraction. Since 2013, he focused his research in the field of reactive bubble columns (SPP1740), in particular on numerical simulation and hydrodynamic/reaction interaction on different scales. He leads projects in the fields of multiphase systems and particle detection. Core areas of his research are multiscale modeling and control, population balance modeling, mass transport, laser-based as well as optical measurement techniques and particle detection. He teaches at TU Kaiserslautern in the fields of computer-aided engineering, environmental process engineering and microprocess engineering. In 2019, he completed his habilitation examination.

Hans-Jörg Bart studied chemical engineering and received his PhD from the University of Technology Graz, Austria. After his habilitation, he became head of the Christian Doppler Laboratory "Modellierung Reaktiver Systeme in der Verfahrenstechnik" and is now a Senior Fellow of the Christian Doppler Society, Vienna. He is Honorary Professor at the Kunming University, China, and since 1994 holds the Chair of Separation Science and Technology at the TU Kaiserslautern.

Symbols used

A	[m^2]	interfacial area
C_D	[–]	drag coefficient
C_L	[–]	lift coefficient
C_{TD}	[–]	turbulent dispersion coefficient
C_{VM}	[–]	virtual mass coefficient
C_W	[–]	wall lubrication coefficient
C_g, C_β	[–]	breakup parameters
C_h, C_λ	[–]	coalescence parameters
$C_{\varepsilon s}$	[–]	turbulence modification exponent
c	[kmol m^{-3}]	molar concentration
c_f	[–]	increase coefficient of surface area
D	[$m^2 s^{-1}$]	diffusion coefficient
D_{col}	[m]	column diameter
d_b	[m]	bubble diameter
$d_{b\parallel}$	[m]	bubble minor axis
$d_{b\perp}$	[m]	bubble major axis
Δd	[m]	bubble size bin width
E	[–]	enhancement factor
E_b	[–]	aspect ratio
Eo	[–]	Eötvös number, Bond number
$\mathbf{F}$	[N]	force vector
f_{vb}	[–]	volume ratio
g	[m s^{-2}]	acceleration due to gravity
g_b	[s^{-1}]	breakup frequency
H	[–]	dimensionless Henry constant
h_c	[$m^3 s^{-1}$]	collision frequency
$\mathbf{I}$	[–]	unity tensor
J_m	[–]	number of species on educt/product side
k	[$m^2 s^{-2}$]	turbulent kinetic energy
k_l	[m s^{-1}]	mass transfer coefficient
k_m	[variable]	reaction rate coefficient (unit depends on reaction order)
M	[–]	total number of reactions
$\dot{m}$	[kg $m^{-3} s^{-1}$]	mass transfer rate
m_b	[kg]	bubble mass
Mo	[–]	Morton number
N	[–]	total number of bubbles
N_S	[–]	number of species
n	[m^{-3}]	number density function
$\mathbf{n}$	[–]	normal vector
p	[Pa]	pressure
r_b	[m]	bubble radius
Re	[–]	particle Reynolds number
Re_ω	[–]	vorticity Reynolds number
$\mathbf{S}$	[s^{-1}]	characteristic filtered rate of strain
$\dot{S}^j$	[kg s^{-1}]	production rate of species j
Sc	[–]	Schmitt number
Sh	[–]	Sherwood number
Sr	[–]	ratio of particle Reynolds number and vorticity Reynolds number
St	[–]	Stokes number
t	[s]	time
t_{ij}	[s]	film drainage time
Ta	[–]	Tadaki number
$\mathbf{u}$	[m s^{-1}]	velocity vector
V	[m^3]	volume of bubble
V'	[m^3]	volume of second bubble
V_{cell}	[m^3]	cell volume
W	[kg $kmol^{-1}$]	molar mass
We_{ij}	[–]	Weber number of two coalescing bubbles
X	[–]	species j in summation formula
$\mathbf{x}$	[m]	position vector
Y	[–]	mass fraction
y_w	[m]	distance between bubble and wall

Greek letters

α	[–]	volume fraction
β	[–]	solid-effect multiplier
β_b	[–]	daughter size distribution
Γ_c	[$m^3 s^{-1}$]	coalescence frequency
Δ_S	[m]	grid width
$\delta(n)$	[–]	delta function of normal coordinate n
ε	[$m^2 s^{-3}$]	dissipation rate of the turbulent kinetic energy
κ	[–]	curvature
λ_c	[–]	coalescence efficiency
λ_ε	[m]	turbulent eddy size
μ	[kg $m^{-1} s^{-1}$]	dynamic viscosity
ν_b	[–]	number of daughter bubbles

ν_m	[–]	stoichiometric coefficient in reaction *m*
ρ	[kg m^{-3}]	mass density
σ	[N m^{-1}]	surface tension
σ_{TD}	[–]	turbulent Schmidt number
τ	[N m^{-2}]	stress tensor
τ_{ij}	[s]	contact time
ω_m	[kmol m^{-3}s^{-1}]	reaction rate

Sub- and Superscripts

b	bubble
BIT	bubble-induced turbulence
CT	Coulaloglou & Tavlarides model
cap	cap bubble
disp	turbulent dispersion
drag	drag
eff	effective
ell	ellipsoidal bubble
g	gas
HI	Hibiki & Ishii model
highRe	high Reynolds numbers
i	phase (gas, liquid, solid), primary bubbles in breakup and coalescence models
j	species, second bubble in breakup and coalescence models
inter	interphase exchange
$L_{1\ldots3}$	Laakkonen model
Luo	Luo model
l	liquid
lift	lift
lowRe	low Reynolds number
m	index of reaction
max	maximum
min	minimum
s	solid
se	solid-effect
sl	slurry
sph	spherical bubble
swarm	swarm effect
turb	turbulent
vm	added-mass, virtual mass
wake	wake-entrainment
wall	wall lubrication
*	gas-liquid interface equilibrium
′	forward reaction (educt)
″	backward reaction (educt)

Abbreviations

2D	2-dimensional
3D	3-dimensional
BIT	bubble-induced turbulence
BSD	bubble size distribution
CFD	computational fluid dynamics
CQMOM	conditional, cumulative quadrature method of moments
CM	classes method
DNS	direct numerical simulation
DQMOM	direct quadrature method of moments
EE	Euler-Euler approach
EL	Euler-Lagrange approach
EQMOM	extended quadrature method of moments
GENTOP	generalized two-phase flow
IATE	interfacial area transport equation
LES	large eddy simulation
OPOSPM	one primary one secondary particle method
PBE	population balance equation
PLIC	piecewise linear interface calculation
QMOM	quadrature method of moments
RANS	Reynolds averaged Navier-Stokes equations
RSM	Reynolds stress model
SGS	sub-grid scale
SLIC	simple line interface calculation
SMM	standard method of moments
SQMOM	sectional quadrature method of moments
VOF	Volume-of-fluid method

References

[1] Y. T. Shah, B. G. Kelkar, S. P. Godbole, W.-D. Deckwer, *AIChE J.* **1982**, *28 (3)*, 353–379. DOI: https://doi.org/10.1002/aic.690280302

[2] W.-D. Deckwer, A. Schumpe, *Chem. Ing. Tech.* **1985**, *57 (9)*, 754–767. DOI: https://doi.org/10.1002/cite.330570909

[3] L.-S. Fan, *Gas-liquid-solid fluidization engineering*, Butterworths series in chemical engineering, Butterworths, Boston **1989**.

[4] *Chem. Ing. Tech.* **2013**, *85 (7)*, 965–1156.

[5] S. Degaleesan, M. Dudukovic, Y. Pan, *AIChE J.* **2001**, *47 (9)*, 1913–1931. DOI: https://doi.org/10.1002/aic.690470904

[6] N. Kantarci, F. Borak, K. O. Ulgen, *Process Biochem.* **2005**, *40 (7)*, 2263–2283. DOI: https://doi.org/10.1016/j.procbio.2004.10.004

[7] S. Schlüter, A. Steiff, P.-M. Weinspach, *Chem. Eng. Process.* **1995**, *34 (3)*, 157–172. DOI: https://doi.org/10.1016/0255-2701(94)04002-8

[8] C. Leonard, J.-H. Ferrasse, O. Boutin, S. Lefevre, A. Viand, *Chem. Eng. Res. Des.* **2015**, *100*, 391–421. DOI: https://doi.org/10.1016/j.cherd.2015.05.013

[9] S. Sideman, Ö. Hortaçsu, J. W. Fulton, *Ind. Eng. Chem.* **1966**, *58 (7)*, 32–47. DOI: https://doi.org/10.1021/ie50679a006

[10] A. Tomiyama, *Multiphase Sci. Technol.* **1998**, *10 (4)*, 369–405. DOI: https://doi.org/10.1615/MultScienTechn.v10.i4.40

[11] H. A. Jakobsen, H. Lindborg, C. A. Dorao, *Ind. Eng. Chem. Res.* **2005**, *44 (14)*, 5107–5151. DOI: https://doi.org/10.1021/ie049447x

[12] T. Wang, *Front. Chem. Sci. Eng.* **2011**, *5 (2)*, 162–172. DOI: https://doi.org/10.1007/s11705-009-0267-5

[13] D. Bothe, M. Schmidtke, H.-J. Warnecke, *Chem. Eng. Technol.* **2006**, *29 (9)*, 1048–1053. DOI: https://doi.org/10.1002/ceat.200600168

[14] R. Krishna, J. M. van Baten, *Int. Commun. Heat Mass Transfer* **1999**, *26 (7)*, 965–974. DOI: https://doi.org/10.1016/S0735-1933(99)00086-X

[15] K. Hayashi, A. Tomiyama, *Int. J. Multiphase Flow* **2012**, *39*, 78–87. DOI: https://doi.org/10.1016/j.ijmultiphaseflow.2011.11.001
[16] S. Fleckenstein, D. Bothe, *Chem. Eng. Sci.* **2013**, *102*, 514–523. DOI: https://doi.org/10.1016/j.ces.2013.08.033
[17] J. Lee, C. Pozrikidis, *Comput. Fluids* **2006**, *35 (1)*, 43–60. DOI: https://doi.org/10.1016/j.compfluid.2004.11.004
[18] Y. Zhang, J. B. McLaughlin, J. A. Finch, *Chem. Eng. Sci.* **2001**, *56 (23)*, 6605–6616. DOI: https://doi.org/10.1016/S0009-2509(01)00304-9
[19] A. Paschedag, W. H. Piarah, M. Kraume, *Chem. Ing. Tech.* **2001**, *73 (11)*, 1431–1435. DOI: https://doi.org/10.1002/1522-2640(200111)73:11<1431:AID-CITE1431>3.0.CO;2-3
[20] C. Wylock, A. Larcy, P. Colinet, T. Cartage, B. Haut, *Colloids Surf., A* **2011**, *381 (1)*, 130–138. DOI: https://doi.org/10.1016/j.colsurfa.2011.03.044
[21] H. Marschall, K. Hinterberger, C. Schüler, F. Habla, O. Hinrichsen, *Chem. Eng. Sci.* **2012**, *78*, 111–127. DOI: https://doi.org/10.1016/j.ces.2012.02.034
[22] A. Esmaeeli, G. Tryggvason, *J. Fluid Mech.* **1998**, *377*, 313–345. DOI: https://doi.org/10.1017/S0022112098003176
[23] G. Tryggvason, A. Esmaeeli, J. Lu, S. Biswas, *Fluid Dyn. Res.* **2006**, *38 (9)*, 660. DOI: https://doi.org/10.1016/j.fluiddyn.2005.08.006
[24] M. van Sint Annaland, N. G. Deen, J. A. M. Kuipers, *Chem. Eng. Sci.* **2005**, *60 (11)*, 2999–3011. DOI: https://doi.org/10.1016/j.ces.2005.01.031
[25] N. Balcázar, O. Lehmkuhl, J. Castro, A. Oliva, in *Direct and large-eddy simulation X*, Vol. 24, ERCOFTAC Series, Vol. 24 (Eds: D. G. E. Grigoriadis et al.), Springer, Cham **2018**.
[26] R. Krishna, J. M. van Baten, *Chem. Eng. Res. Des.* **2001**, *79 (3)*, 283–309. DOI: https://doi.org/10.1205/026387601750281815
[27] N. Balcázar, J. Castro, J. Rigola, A. Oliva, *Procedia Comput. Sci.* **2017**, *108*, 2008–2017. DOI: https://doi.org/10.1016/j.procs.2017.05.076
[28] N. Balcázar-Arciniega, J. Rigola, A. Oliva, in *Computational Science – ICCS 2019: 19th International Conference* (Eds: J. M. F. Rodrigues), Springer, Cham **2019**.
[29] A. Esmaeeli, G. Tryggvason, *J. Fluid Mech.* **1999**, *385*, 325–358. DOI: https://doi.org/10.1017/S0022112099004310
[30] G. Tryggvason, B. Bunner, A. Esmaeeli, D. Juric, N. Al-Rawahi, W. Tauber, J. Han, S. Nas, Y.-J. Jan, *J. Comput. Phys.* **2001**, *169 (2)*, 708–759. DOI: https://doi.org/10.1006/jcph.2001.6726
[31] S. Radl, G. Tryggvason, J. G. Khinast, *AIChE J.* **2007**, *53 (7)*, 1861–1878. DOI: https://doi.org/10.1002/aic.11211
[32] J. A. Sethian, *Level set methods and fast marching methods: evolving interfaces in computational geometry, fluid mechanics, computer vision, and materials science*, Cambridge University Press, Cambridge **1999**.
[33] Y. C. Chang, T. Y. Hou, B. Merriman, S. Osher, *J. Comput. Phys.* **1996**, *124 (2)*, 449–464. DOI: https://doi.org/10.1006/jcph.1996.0072
[34] M. Sussman, A. S. Almgren, J. B. Bell, P. Colella, L. H. Howell, M. L. Welcome, *J. Comput. Phys.* **1999**, *148 (1)*, 81–124. DOI: https://doi.org/10.1006/jcph.1998.6106
[35] R. Croce, M. Griebel, M. A. Schweitzer, *Int. J. Numer. Meth. Fluids* **2010**, *62 (9)*, 963–993. DOI: https://doi.org/10.1002/fld.2051
[36] M. Ida, *Comput. Phys. Commun.* **2000**, *132 (1)*, 44–65. DOI: https://doi.org/10.1016/S0010-4655(00)00136-3
[37] J. E. Welch, F. H. Harlow, J. P. Shannon, B. J. Daly, *The MAC method-a computing technique for solving viscous, incompressible, transient fluid-flow problems involving free surfaces*, Los Alamos Scientific Lab. Report LA-3425, **1965**.
[38] M. W. Hlawitschka, S. Tiwari, J. Kwizera, A. Klar, H.-J. Bart, *Simulation of Fluid Particle Cutting – Validation and Case Study* **2017**. http://arxiv.org/abs/1709.01729
[39] W. F. Noh, P. Woodward, in *Proc. of the 5th Int. Conf. Numerical Methods in Fluid Dynamics*, Lecture Notes in Physics, Vol. 59 (Eds: A. I. Vooren, P. J. Zandbergen), Springer, Berlin **1976**.
[40] W. Rider, D. Kothe, in *Proc. of the 12th Computational Fluid Dynamics Conference*, American Institute of Aeronautics and Astronautics, Reston, VA **1995**.
[41] K. Ito, T. Kunugi, H. Ohshima, T. Kawamura, *Comput. Fluids* **2013**, *88*, 250–261. DOI: https://doi.org/10.1016/j.compfluid.2013.09.016
[42] M. Huang, L. Wu, B. Chen, *Numer. Heat Transfer, Part B* **2012**, *61 (5)*, 412–437. DOI: https://doi.org/10.1080/10407790.2012.672818
[43] D. Deising, D. Bothe, H. Marschall, *Comput. Fluids* **2018**, *172*, 524–537. DOI: https://doi.org/10.1016/j.compfluid.2018.03.041
[44] A. J. C. Ladd, *J. Fluid Mech.* **1994**, *271*, 285–309. DOI: https://doi.org/10.1017/S0022112094001771
[45] A. J. C. Ladd, *J. Fluid Mech.* **1994**, *271*, 311–339. DOI: https://doi.org/10.1017/S0022112094001783
[46] C. Janssen, M. Krafczyk, *Comput. Math. Appl.* **2010**, *59 (7)*, 2215–2235. DOI: https://doi.org/10.1016/j.camwa.2009.08.064
[47] K. Sankaranarayanan, X. Shan, I. G. Kevrekidis, S. Sundaresan, *J. Fluid Mech.* **2002**, *452*, 61–96. DOI: https://doi.org/10.1017/S0022112001006619
[48] K. Sankaranarayanan, S. Sundaresan, *Chem. Eng. Sci.* **2002**, *57 (17)*, 3521–3542. DOI: https://doi.org/10.1016/S0009-2509(02)00269-5
[49] R. Rzehak, S. Kriebitzsch, *Int. J. Multiphase Flow* **2015**, *68*, 135–152. DOI: https://doi.org/10.1016/j.ijmultiphaseflow.2014.09.005
[50] M. Ishii, K. Mishima, *Nucl. Eng. Des.* **1984**, *82 (2)*, 107–126. DOI: https://doi.org/10.1016/0029-5493(84)90207-3
[51] L. Schiller, A. Naumann, *VDI Zeitung* **1935**, *77*, 318–320.
[52] R. Clift, J. R. Grace, M. E. Weber, *Bubbles, drops, and particles*, Academic Press, New York **1978**.
[53] M. Ishii, N. Zuber, *AIChE J.* **1979**, *25 (5)*, 843–855. DOI: https://doi.org/10.1002/aic.690250513
[54] A. Tomiyama, I. Kataoka, I. Zun, T. Sakaguchi, *JSME Int. J., Ser. B* **1998**, *41 (2)*, 472–479. DOI: https://doi.org/10.1299/jsmeb.41.472
[55] S. Laín, D. Bröder, M. Sommerfeld, M. F. Göz, *Int. J. Multiphase Flow* **2002**, *28 (8)*, 1381–1407. DOI: https://doi.org/10.1016/S0301-9322(02)00028-9
[56] A. Tomiyama, I. Kataoka, T. Fukuda, T. Sakaguchi, *Trans. Jpn. Soc. Mech. Eng., B* **1995**, *61 (588)*, 2810–2817. DOI: https://doi.org/10.1299/kikaib.61.2810
[57] H. Rusche, Issa R. I., in *Proc. of the Japanese European Two-Phase Flow Meeting*, Tshkuba, Japan **2000**.
[58] I. Roghair, Y. M. Lau, N. G. Deen, H. M. Slagter, M. W. Baltussen, M. van Sint Annaland, J. A. M. Kuipers, *Chem. Eng. Sci.* **2011**, *66 (14)*, 3204–3211. DOI: https://doi.org/10.1016/j.ces.2011.02.030
[59] D. Legendre, J. Magnaudet, *J. Fluid Mech.* **1998**, *368*, 81–126. DOI: https://doi.org/10.1017/S0022112098001621
[60] A. Tomiyama, H. Tamai, I. Zun, S. Hosokawa, *Chem. Eng. Sci.* **2002**, *57 (11)*, 1849–1858. DOI: https://doi.org/10.1016/S0009-2509(02)00085-4
[61] R. M. Wellek, A. K. Agrawal, A. H. P. Skelland, *AIChE J.* **1966**, *12 (5)*, 854–862. DOI: https://doi.org/10.1002/aic.690120506
[62] I. A. Vakhrushev, G. I. Efremov, *Chem. Technol. Fuels Oils* **1970**, *6 (5)*, 376–379. DOI: https://doi.org/10.1007/BF01171684

[63] S. P. Antal, R. T. Lahey, J. E. Flaherty, *Int. J. Multiphase Flow* **1991**, *17 (5)*, 635–652. DOI: https://doi.org/10.1016/0301-9322(91)90029-3
[64] S. Hosokawa, A. Tomiyama, S. Misaki, T. Hamada, in *Proc. of the 2002 ASME Joint U.S.-European Fluids Engineering Conference* (Eds: U. S. Rohatgi), American Society of Mechanical Engineers, New York **2002**.
[65] T. Frank, in *Proc. of the NAFEMS Seminar*, Niedernhausen/Wiesbaden **2005**.
[66] R. T. Lahey, M. Lopez de Bertodano, O. C. Jones, *Nucl. Eng. Des.* **1993**, *141 (1)*, 177–201. DOI: https://doi.org/10.1016/0029-5493(93)90101-E
[67] A. D. Burns, T. Frank, I. Hamill, J. M. Shi, in *Proc. of the 5th Int. Conf. Multiphase Flow (ICMF)*, Yokohama **2004**.
[68] D. Lucas, E. Krepper, H.-M. Prasser, *Chem. Eng. Sci.* **2007**, *62 (15)*, 4146–4157. DOI: https://doi.org/10.1016/j.ces.2007.04.035
[69] M. A. Lopez de Bertodano, *Nucl. Eng. Des.* **1998**, *179 (1)*, 65–74. DOI: https://doi.org/10.1016/S0029-5493(97)00244-6
[70] M. Lopez de Bertodano, F. J. Moraga, D. A. Drew, R. T. Lahey, *Int. J. Multiphase Flow* **2004**, *126 (4)*, 573. DOI: https://doi.org/10.1115/1.1777231
[71] D. Zhang, N. G. Deen, J. A. M. Kuipers, *Chem. Eng. Sci.* **2006**, *61 (23)*, 7593–7608. DOI: https://doi.org/10.1016/j.ces.2006.08.053
[72] M. Simcik, M. C. Ruzicka, J. Drahoš, *Chem. Eng. Sci.* **2008**, *63 (18)*, 4580–4595. DOI: https://doi.org/10.1016/j.ces.2008.06.011
[73] M. J. Prince, H. W. Blanch, *AIChE J.* **1990**, *36 (10)*, 1485–1499. DOI: https://doi.org/10.1002/aic.690361004
[74] H. Luo, H. F. Svendsen, *AIChE J.* **1996**, *42 (5)*, 1225–1233. DOI: https://doi.org/10.1002/aic.690420505
[75] F. Lehr, M. Millies, D. Mewes, *AIChE J.* **2002**, *48 (11)*, 2426–2443. DOI: https://doi.org/10.1002/aic.690481103
[76] M. Laakkonen, V. Alopaeus, J. Aittamaa, *Chem. Eng. Sci.* **2006**, *61 (1)*, 218–228. DOI: https://doi.org/10.1016/j.ces.2004.11.066
[77] C. A. Coulaloglou, L. L. Tavlarides, *Chem. Eng. Sci.* **1977**, *32 (11)*, 1289–1297. DOI: https://doi.org/10.1016/0009-2509(77)85023-9
[78] H. Luo, *Coalescence, Breakup, and Circulation in Bubble Column Reactors*, PhD Thesis, Norwegian University of Science and Technology, Trondheim **1993**.
[79] T. Wang, J. Wang, Y. Jin, *Chem. Eng. Sci.* **2005**, *60 (22)*, 6199–6209. DOI: https://doi.org/10.1016/j.ces.2005.04.027
[80] T. Hibiki, M. Ishii, *Int. J. Heat Mass Transfer* **2002**, *45 (11)*, 2351–2372. DOI: https://doi.org/10.1016/S0017-9310(01)00327-1
[81] Y. Liao, D. Lucas, *Chem. Eng. Sci.* **2009**, *64 (15)*, 3389–3406. DOI: https://doi.org/10.1016/j.ces.2009.04.026
[82] Y. Liao, D. Lucas, *Chem. Eng. Sci.* **2010**, *65 (10)*, 2851–2864. DOI: https://doi.org/10.1016/j.ces.2010.02.020
[83] M. J. Hounslow, R. L. Ryall, V. R. Marshall, *AIChE J.* **1988**, *34 (11)*, 1821–1832. DOI: https://doi.org/10.1002/aic.690341108
[84] J. D. Lister, D. J. Smit, M. J. Hounslow, *AIChE J.* **1995**, *41 (3)*, 591–603. DOI: https://doi.org/10.1002/aic.690410317
[85] D. Ramkrishna, *Population balances: Theory and applications to particulate systems in engineering*, Academic Press, New York **2000**.
[86] P. Chen, J. Sanyal, M. P. Dudukovic, *Chem. Eng. Sci.* **2004**, *59 (22)*, 5201–5207. DOI: https://doi.org/10.1016/j.ces.2004.07.037
[87] J. Sanyal, D. L. Marchisio, R. O. Fox, K. Dhanasekharan, *Ind. Eng. Chem. Res.* **2005**, *44 (14)*, 5063–5072. DOI: https://doi.org/10.1021/ie049555j
[88] T. Frank, P. J. Zwart, J. Shi, E. Krepper, D. Lucas, U. Rohde, in *Proc. of the Int. Conf. Nuclear Energy for New Europe* (Eds: B. Mavko, I. Kljenak). Ljubljana, Slovenia **2005**.
[89] M. R. Bhole, J. B. Joshi, D. Ramkrishna, *Chem. Eng. Sci.* **2008**, *63 (8)*, 2267–2282. DOI: https://doi.org/10.1016/j.ces.2008.01.013
[90] H. M. Hulburt, S. Katz, *Chem. Eng. Sci.* **1964**, *19 (8)*, 555–574. DOI: https://doi.org/10.1016/0009-2509(64)85047-8
[91] R. McGraw, *Aerosol Sci. Technol.* **1997**, *27 (2)*, 255–265. DOI: https://doi.org/10.1080/02786829708965471
[92] D. L. Marchisio, J. T. Pikturna, R. O. Fox, R. D. Vigil, A. A. Barresi, *AIChE J.* **2003**, *49 (5)*, 1266–1276. DOI: https://doi.org/10.1002/aic.690490517
[93] P. L. C. Lage, *Comput. Chem. Eng.* **2011**, *35 (11)*, 2186–2203. DOI: https://doi.org/10.1016/j.compchemeng.2011.05.017
[94] D. L. Marchisio, R. O. Fox, *J. Aerosol Sci.* **2005**, *36 (1)*, 43–73. DOI: https://doi.org/10.1016/j.jaerosci.2004.07.009
[95] M. W. Hlawitschka, J. Schäfer, M. Hummel, C. Garth, H.-J. Bart, *Chem. Ing. Tech.* **2016**, *88 (10)*, 1480–1491. DOI: https://doi.org/10.1002/cite.201600006
[96] C. Yuan, R. O. Fox, *J. Comput. Phys.* **2011**, *230 (22)*, 8216–8246. DOI: https://doi.org/10.1016/j.jcp.2011.07.020
[97] M. Attarakih, *Comput. Chem. Eng.* **2013**, *48*, 1–13. DOI: https://doi.org/10.1016/j.compchemeng.2012.08.001
[98] C. Yuan, F. Laurent, R. O. Fox, *J. Aerosol Sci.* **2012**, *51*, 1–23. DOI: https://doi.org/10.1016/j.jaerosci.2012.04.003
[99] E. A. Mahvelati, G. S.-P. Lemieux, C. B. Vieira, G. Litrico, P. Proulx, in *AIP Conference Proceedings 1978*, Thessaloniki, Greece **2018**.
[100] M. M. Attarakih, C. Drumm, H.-J. Bart, Faqir N. M., in *Proc. of the 3rd Int. Conf. on Population Balance Modelling*, Quebec **2007**.
[101] J. Schäfer, M. W. Hlawitschka, M. M. Attarakih, H.-J. Bart, *AIChE J.* **2019**, *65 (10)*, e16694. DOI: https://doi.org/10.1002/aic.16694
[102] M. M. Attarakih, M. Jaradat, C. Drumm, H.-J. Bart, S. Tiwari, V. K. Sharma, J. Kuhnert, A. Klar, *Comput. Aid. Chem. Eng.* **2009**, *26*, 1333–1338.
[103] M. Ishii, S. Kim, J. Uhle, *Int. J. Heat Mass Transfer* **2002**, *45 (15)*, 3111–3123. DOI: https://doi.org/10.1016/S0017-9310(02)00041-8.
[104] S. Hänsch, D. Lucas, E. Krepper, T. Höhne, *Int. J. Multiphase Flow* **2012**, *47*, 171–182. DOI: https://doi.org/10.1016/j.ijmultiphaseflow.2012.07.007
[105] M. Hummel, L. Jöckel, J. Schäfer, M. W. Hlawitschka, C. Garth, in *Physical Modeling for Virtual Manufacturing Systems and Processes*, Vol. 869 (Eds: J. C. Aurich et al.), Trans Tech Publications, Zurich **2017**.
[106] M. Hummel, L. Jöckel, J. Schäfer, M. W. Hlawitschka, C. Garth, *Comput. Graphics Forum* **2017**, *36 (3)*, 469–477. DOI: https://doi.org/10.1111/cgf.13203
[107] M. W. Hlawitschka, J. Schäfer, L. Jöckel, M. Hummel, C. Garth, H.-J. Bart, *J. Chem. Eng. Jpn.* **2018**, *51 (4)*, 356–365. DOI: https://doi.org/10.1252/jcej.17we290
[108] A. Weber, H.-J. Bart, *Open Chem. Eng. J.* **2018**, *12 (1)*, 1–13. DOI: https://doi.org/10.2174/1874123101812010001
[109] D. Darmana, N. G. Deen, J. A. M. Kuipers, in *Proc. of the 5th Int. Conf. Multiphase Flow (ICMF)*, Yokohama **2004**.
[110] D. Darmana, N. G. Deen, J. A. M. Kuipers, *Chem. Eng. Sci.* **2005**, *60 (12)*, 3383–3404. DOI: https://doi.org/10.1016/j.ces.2005.01.025
[111] D. Darmana, N. G. Deen, J. A. M. Kuipers, *J. Comput. Phys.* **2006**, *220 (1)*, 216–248. DOI: https://doi.org/10.1016/j.jcp.2006.05.011
[112] D. Darmana, R. L. B. Henket, N. G. Deen, J. A. M. Kuipers, *Chem. Eng. Sci.* **2007**, *62 (9)*, 2556–2575. DOI: https://doi.org/10.1016/j.ces.2007.01.065
[113] A. Tomiyama, G. P. Celata, S. Hosokawa, S. Yoshida, *Int. J. Multiphase Flow* **2002**, *28 (9)*, 1497–1519. DOI: https://doi.org/10.1016/S0301-9322(02)00032-0

[114] A. Weber, H.-J. Bart, A. Klar, *Open J. Fluid Dyn.* **2017**, *07 (03)*, 288–309. DOI: https://doi.org/10.4236/ojfd.2017.73019
[115] M. Sommerfeld, *Int. J. Multiphase Flow* **2001**, *27 (10)*, 1829–1858. DOI: https://doi.org/10.1016/S0301-9322(01)00035-0
[116] A. Vikhansky, M. Kraft, *Chem. Eng. Sci.* **2004**, *59 (13)*, 2597–2606. DOI: https://doi.org/10.1016/j.ces.2004.02.016
[117] M. C. Gruber, S. Radl, J. G. Khinast, *Chem. Ing. Tech.* **2013**, *85 (7)*, 1118–1130. DOI: https://doi.org/10.1002/cite.201300024
[118] D. Jain, J. A. M. Kuipers, N. G. Deen, *Chem. Eng. Sci.* **2015**, *137*, 685–696. DOI: https://doi.org/10.1016/j.ces.2015.07.025
[119] R. Sungkorn, J. J. Derksen, J. G. Khinast, *Int. Commun. Heat Mass Transfer* **2012**, *36*, 153–166. DOI: https://doi.org/10.1016/j.ijheatfluidflow.2012.04.006
[120] S. Schwarz, T. Kempe, J. Fröhlich, *J. Comput. Phys.* **2016**, *315*, 124–149. DOI: https://doi.org/10.1016/j.jcp.2016.01.033
[121] Z. Khan, V. H. Bhusare, J. B. Joshi, *Chem. Eng. Sci.* **2017**, *164*, 34–52. DOI: https://doi.org/10.1016/j.ces.2017.01.023
[122] J. Smagorinsky, *Mon. Wea. Rev.* **1963**, *91 (3)*, 99–164. DOI: https://doi.org/10.1175/1520-0493(1963)091<0099:GCEWTP>2.3.CO;2
[123] N. G. Deen, T. Solberg, B. H. Hjertager, *Chem. Eng. Sci.* **2001**, *56 (21)*, 6341–6349. DOI: https://doi.org/10.1016/S0009-2509(01)00249-4
[124] M. T. Dhotre, N. G. Deen, B. Niceno, Z. Khan, J. B. Joshi, *Int. J. Chem. Eng.* **2013**, *2013 (2)*, 1–22. DOI: https://doi.org/10.1155/2013/343276
[125] Y. Sato, K. Sekoguchi, *Int. J. Multiphase Flow* **1975**, *2 (1)*, 79–95. DOI: https://doi.org/10.1016/0301-9322(75)90030-0
[126] D. Pfleger, S. Becker, *Chem. Eng. Sci.* **2001**, *56 (4)*, 1737–1747. DOI: https://doi.org/10.1016/S0009-2509(00)00403-6
[127] A. A. Troshko, Y. A. Hassan, *Int. J. Multiphase Flow* **2001**, *27 (11)*, 1965–2000. DOI: https://doi.org/10.1016/S0301-9322(01)00043-X
[128] R. Rzehak, E. Krepper, *Int. J. Multiphase Flow* **2013**, *55*, 138–155. DOI: https://doi.org/10.1016/j.ijmultiphaseflow.2013.04.007
[129] T. Ma, C. Santarelli, T. Ziegenhein, D. Lucas, J. Fröhlich, *Phys. Rev. Fluids* **2017**, *2 (3)*, 34301. DOI: https://doi.org/10.1103/PhysRevFluids.2.034301
[130] M. R. Bhole, S. Roy, J. B. Joshi, *Ind. Eng. Chem. Res.* **2006**, *45 (26)*, 9201–9207. DOI: https://doi.org/10.1021/ie060745z
[131] M. T. Dhotre, B. Niceno, B. L. Smith, *Chem. Eng. J.* **2008**, *136 (2)*, 337–348. DOI: https://doi.org/10.1016/j.cej.2007.04.016
[132] P. Renze, A. Buffo, D. L. Marchisio, M. Vanni, *Chem. Ing. Tech.* **2014**, *86 (7)*, 1088–1098. DOI: https://doi.org/10.1002/cite.201400004
[133] B. Magolan, N. Lubchenko, E. Baglietto, *Chem. Eng. Sci.* **2019**, *2*, 100009. DOI: https://doi.org/10.1016/j.cesx.2019.100009
[134] T. T. Liu, *Experimental investigation of turbulence structure in two-phase bubbly flow*, PhD Thesis, Northwestern Univ., Evanston **1989**.
[135] J. Parekh, R. Rzehak, *Int. J. Multiphase Flow* **2018**, *99*, 231–245. DOI: https://doi.org/10.1016/j.ijmultiphaseflow.2017.10.012
[136] M. W. Hlawitschka, P. Kováts, K. Zähringer, H.-J. Bart, *Chem. Eng. Sci.* **2017**, *170*, 306–319. DOI: https://doi.org/10.1016/j.ces.2016.12.053
[137] A. Buffo, M. Vanni, D. L. Marchisio, *Appl. Math. Modell.* **2017**, *44*, 43–60. DOI: https://doi.org/10.1016/j.apm.2016.11.010
[138] A. Weber, *Simulating bubble movement with the Euler-Lagrange approach*, PhD Thesis, Technische Universität Kaiserslautern, Verlag Dr. Hut, München **2018**.
[139] M. C. Gruber, S. Radl, J. G. Khinast, *Chem. Eng. Sci.* **2015**, *137*, 188–204. DOI: https://doi.org/10.1016/j.ces.2015.06.008
[140] R. B. Bird, W. E. Stewart, E. N. Lightfoot, *Transport Phenomena*, John Wiley and Sons, Hoboken, NJ **2007**.
[141] R. Krishna, J. W. A. de Swart, J. Ellenberger, G. B. Martina, C. Maretto, *AIChE J.* **1997**, *43 (2)*, 311–316. DOI: https://doi.org/10.1002/aic.690430204
[142] H. Li, A. Prakash, *Powder Technol.* **2000**, *113 (1)*, 158–167. DOI: https://doi.org/10.1016/S0032-5910(00)00228-X
[143] X. Luo, D. J. Lee, R. Lau, G. Yang, L.-S. Fan, *AIChE J.* **1999**, *45 (4)*, 665–680. DOI: https://doi.org/10.1002/aic.690450402
[144] A. Behkish, R. Lemoine, R. Oukaci, B. I. Morsi, *Chem. Eng. J.* **2006**, *115 (3)*, 157–171. DOI: https://doi.org/10.1016/j.cej.2005.10.006
[145] A. R. Sarhan, J. Naser, G. Brooks, *Particuology* **2018**, *36*, 82–95. DOI: https://doi.org/10.1016/j.partic.2017.04.011
[146] M. van der Zon, P. J. Hamersma, E. K. Poels, A. Bliek, *Chem. Eng. Sci.* **2002**, *57 (22)*, 4845–4853. DOI: https://doi.org/10.1016/S0009-2509(02)00281-6
[147] S. Ojima, K. Hayashi, A. Tomiyama, *Int. J. Multiphase Flow* **2014**, *58*, 154–167. DOI: https://doi.org/10.1016/j.ijmultiphaseflow.2013.09.005
[148] L.-S. Fan, O. Hemminger, Z. Yu, F. Wang, *Ind. Eng. Chem. Res.* **2007**, *46 (12)*, 4341–4346. DOI: https://doi.org/10.1021/ie061532c
[149] C. O. Vandu, R. Krishna, *Chem. Eng. Process.* **2004**, *43 (8)*, 987–995. DOI: https://doi.org/10.1016/j.cep.2003.09.007
[150] M. Schlüter, S. Scheid, S. John, N. Räbiger, *J. Chem. Eng. Jpn.* **2004**, *37 (8)*, 947–954. DOI: https://doi.org/10.1252/jcej.37.947
[151] E. Bourloutski, M. Sommerfeld, in *Bubbly Flows*, Vol. 72, Heat and Mass Transfer (Eds: D. Mewes, F. Mayinger, M. Sommerfeld), Springer, Berlin **2004**.
[152] K. D. Squires, J. K. Eaton, *J. Fluids Eng.* **1994**, *116 (4)*, 778. DOI: https://doi.org/10.1115/1.2911849
[153] V. Michele, H. Dziallas, D. C. Hempel, in *Proc. of the ICHMT Int. Symp. on Multiphase Flow and Transport Phenomena*, Antalya **2000**.
[154] D. Matonis, D. Gidaspow, M. Bahary, *AIChE J.* **2002**, *48 (7)*, 1413–1429. DOI: https://doi.org/10.1002/aic.690480706
[155] S. Rabha, M. Schubert, U. Hampel, *Chem. Ing. Tech.* **2013**, *85 (7)*, 1092–1098. DOI: https://doi.org/10.1002/cite.201200227
[156] A. A. Troshko, F. Zdravistch, *Chem. Eng. Sci.* **2009**, *64 (5)*, 892–903. DOI: https://doi.org/10.1016/j.ces.2008.10.022
[157] A. A. Kulkarni, J. B. Joshi, D. Ramkrishna, *AIChE J.* **2004**, *50 (12)*, 3068–3084. DOI: https://doi.org/10.1002/aic.10274
[158] Y. Wu, D. Gidaspow, *Chem. Eng. Sci.* **2000**, *55 (3)*, 573–587. DOI: https://doi.org/10.1016/S0009-2509(99)00313-9
[159] L. Xu, Z. Xia, X. Guo, C. Chen, *Ind. Eng. Chem. Res.* **2014**, *53 (12)*, 4922–4930. DOI: https://doi.org/10.1021/ie403453h
[160] B. Gandhi, A. Prakash, M. A. Bergougnou, *Powder Technol.* **1999**, *103 (2)*, 80–94. DOI: https://doi.org/10.1016/S0032-5910(98)00182-X
[161] X. Zhang, G. Ahmadi, *Chem. Eng. Sci.* **2005**, *60 (18)*, 5089–5104. DOI: https://doi.org/10.1016/j.ces.2005.04.033
[162] E. Delnoij, J. A. M. Kuipers, W. P. M. van Swaaij, *Chem. Eng. Sci.* **1997**, *52 (21)*, 3759–3772. DOI: https://doi.org/10.1016/S0009-2509(97)00222-4
[163] R. Zhou, N. Yang, J. Li, *Powder Technol.* **2017**, *314*, 466–479. DOI: https://doi.org/10.1016/j.powtec.2016.09.083
[164] N. Rados, *Slurry bubble column hydrodynamics: experimentation and modeling*, PhD Thesis, Washington University, St. Louis **2003**.
[165] K. Tsuchiya, A. Furumoto, L.-S. Fan, J. Zhang, *Chem. Eng. Sci.* **1997**, *52 (18)*, 3053–3066. DOI: https://doi.org/10.1016/S0009-2509(97)00127-9
[166] S. Ojima, S. Sasaki, K. Hayashi, A. Tomiyama, *J. Chem. Eng. Jpn.* **2015**, *48 (3)*, 181–189. DOI: https://doi.org/10.1252/jcej.14we248

DOI: 10.1002/cite.201900109

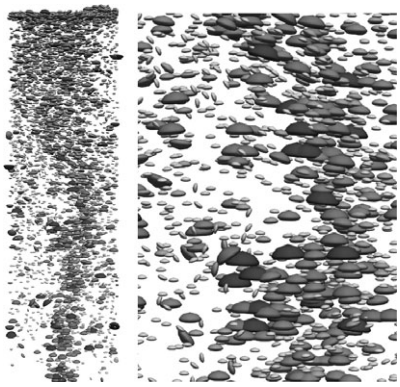

Models for the Numerical Simulation of Bubble Columns: A Review

*A. Mühlbauer, M. W. Hlawitschka, H.-J. Bart**

Review: This review about the developed models for bubble column simulations coupled with CFD methods shows how multiphase, population balance, turbulence, mass transfer and reaction kinetic models are coupled. A special chapter discusses the effects of solids in slurry bubble columns and the modeling approaches.

